Article

An LKB1–mitochondria axis controls T$_H$17 effector function

Francesc Baixauli[1], Klara Piletic[1,7], Daniel J. Puleston[1,7], Matteo Villa[1,7], Cameron S. Field[1], Lea J. Flachsmann[1], Andrea Quintana[1], Nisha Rana[1], Joy Edwards-Hicks[1], Mai Matsushita[1], Michal A. Stanczak[1], Katarzyna M. Grzes[1], Agnieszka M. Kabat[1], Mario Fabri[1,2], George Caputa[1], Beth Kelly[1], Mauro Corrado[1], Yaarub Musa[1], Katarzyna J. Duda[1], Gerhard Mittler[1], David O'Sullivan[1], Hiromi Sesaki[3], Thomas Jenuwein[1], Joerg M. Buescher[1], Edward J. Pearce[1,4,5], David E. Sanin[1,4] & Erika L. Pearce[1,4,6 ✉]

CD4$^+$ T cell differentiation requires metabolic reprogramming to fulfil the bioenergetic demands of proliferation and effector function, and enforce specific transcriptional programmes[1–3]. Mitochondrial membrane dynamics sustains mitochondrial processes[4], including respiration and tricarboxylic acid (TCA) cycle metabolism[5], but whether mitochondrial membrane remodelling orchestrates CD4$^+$ T cell differentiation remains unclear. Here we show that unlike other CD4$^+$ T cell subsets, T helper 17 (T$_H$17) cells have fused mitochondria with tight cristae. T cell-specific deletion of optic atrophy 1 (OPA1), which regulates inner mitochondrial membrane fusion and cristae morphology[6], revealed that T$_H$17 cells require OPA1 for its control of the TCA cycle, rather than respiration. OPA1 deletion amplifies glutamine oxidation, leading to impaired NADH/NAD$^+$ balance and accumulation of TCA cycle metabolites and 2-hydroxyglutarate—a metabolite that influences the epigenetic landscape[5,7]. Our multi-omics approach revealed that the serine/threonine kinase liver-associated kinase B1 (LKB1) couples mitochondrial function to cytokine expression in T$_H$17 cells by regulating TCA cycle metabolism and transcriptional remodelling. Mitochondrial membrane disruption activates LKB1, which restrains IL-17 expression. LKB1 deletion restores IL-17 expression in T$_H$17 cells with disrupted mitochondrial membranes, rectifying aberrant TCA cycle glutamine flux, balancing NADH/NAD$^+$ and preventing 2-hydroxyglutarate production from the promiscuous activity of the serine biosynthesis enzyme phosphoglycerate dehydrogenase (PHGDH). These findings identify OPA1 as a major determinant of T$_H$17 cell function, and uncover LKB1 as a sensor linking mitochondrial cues to effector programmes in T$_H$17 cells.

Mitochondrial function is linked to mitochondrial membrane morphology[4]. Remodelling of the inner mitochondrial membrane and outer mitochondrial membrane (OMM) is coordinated by several GTPases that control the opposing and dynamic processes of mitochondrial fusion and fission[8] (division). Mitochondrial membrane rearrangements sustain mitochondrial function by altering cristae architecture, respiratory complex organization, mtDNA metabolism and organelle distribution[8]. Mitochondrial membrane remodelling is especially relevant during metabolic or environmental fluctuations[9] and diverse signalling pathways regulate pro-fusion and pro-fission proteins to shape mitochondrial structure and support metabolic adaptations. Conversely, mitochondria and mitochondrial membrane remodelling participate in intracellular signalling events, modulating transcription and epigenetics during cell differentiation, immune responses, tumour angiogenesis and cell death[4,10,11]. Given the role of mitochondrial membrane dynamics and metabolism in cell function, we investigated how mitochondrial membrane morphology affects CD4$^+$ T cell differentiation.

T$_H$17 cells have fused mitochondria

We polarized naive CD4$^+$ T (T$_N$) cells expressing a mitochondria-targeted fluorescent protein, into T$_H$1, T$_H$2, T$_H$17 and T regulatory (T$_{reg}$) cell subsets in vitro and assessed their mitochondrial morphology. T$_H$17 cells contained elongated mitochondria with tight cristae (Fig. 1a and Extended Data Fig. 1a,b). Although in vitro-generated T$_H$1 and T$_H$2 cells had increased mitochondrial content and cell size compared with T$_H$17 and T$_{reg}$ cells, all cells had similar amounts of proteins associated with

[1]Max Planck Institute for Immunobiology and Epigenetics, Freiburg, Germany. [2]University of Cologne, Department of Dermatology, Cologne, Germany. [3]Department of Cell Biology, Johns Hopkins University School of Medicine, Baltimore, MD, USA. [4]Department of Oncology, The Bloomberg–Kimmel Institute for Cancer Immunotherapy, Johns Hopkins University, Baltimore, MD, USA. [5]Department Molecular Microbiology and Immunology, Johns Hopkins Bloomberg School of Public Health, Baltimore, MD, USA. [6]Department of Biochemistry and Molecular Biology, Johns Hopkins Bloomberg School of Public Health, Baltimore, MD, USA. [7]These authors contributed equally: Klara Piletic, Daniel J. Puleston, Matteo Villa. ✉e-mail: epearce6@jhmi.edu
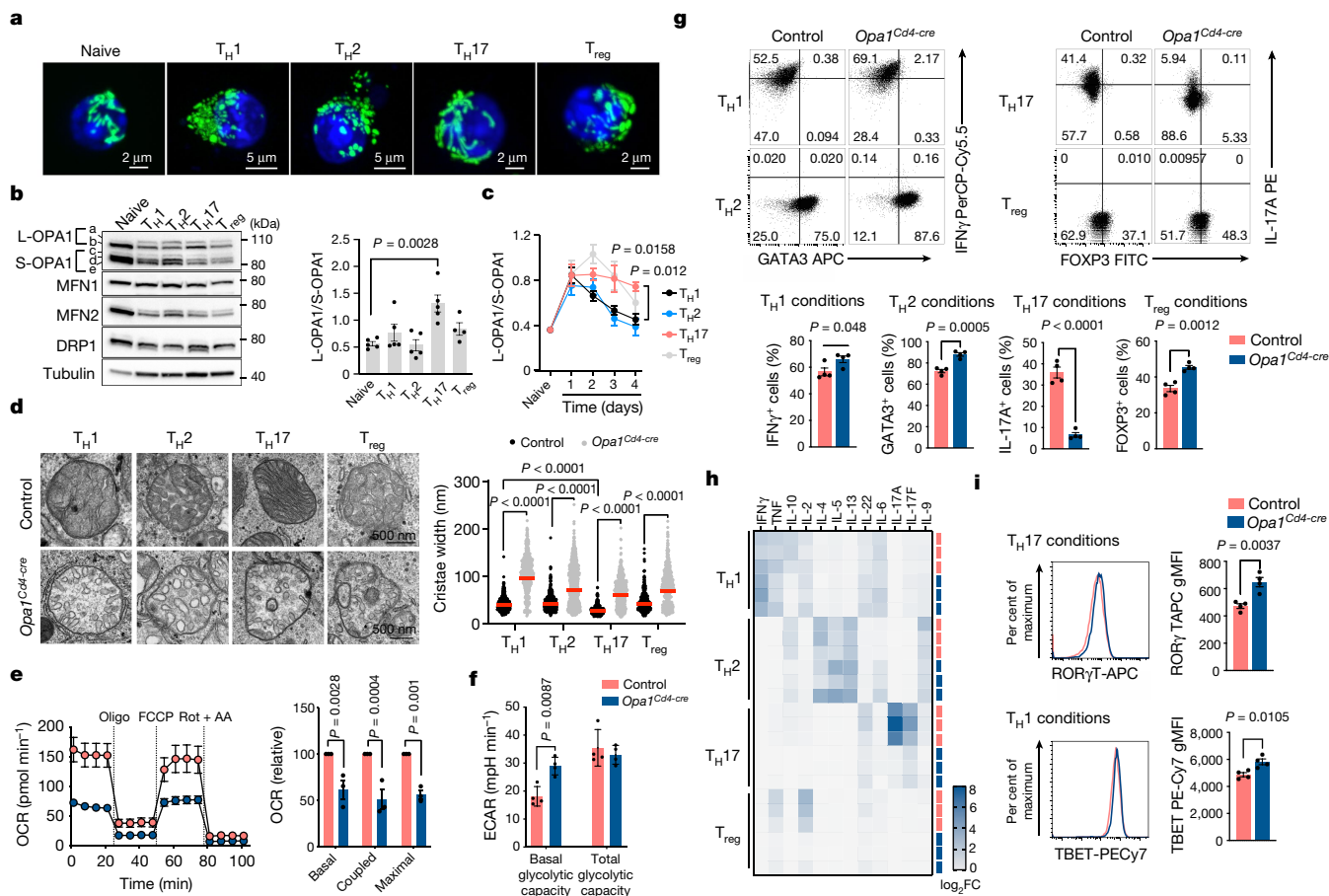
Fig. 1 | OPA1 is required for T_H17 cell effector function. a, Representative live-cell spinning disk microscopy images showing mitochondria (GFP, green) and nuclei (Hoechst 42, blue) in CD4⁺ T cells from PhAM mice cultured in T helper (T_H) and T_reg cell conditions on day 4. Two separate experiments. **b**, Immunoblot of OPA1, MFN2, MFN1, DRP1 (left) and ratio of l- and s-OPA1 isoforms (right) in T_N, T_H and T_reg T cells on day 4. Tubulin is used as a sample processing control. **c**, Kinetics of OPA1 isoforms during T_H and T_reg differentiation. In **b,c**, T_H1, T_H2 and T_H17: $n = 5$ biological replicates, T_reg: $n = 4$ biological replicates and 3 independent experiments. **d**, Electron microscopy (left) and width of mitochondrial cristae (right). Control T_H1: $n = 442$, control T_H2: $n = 401$, control T_H17: $n = 418$, control T_reg: $n = 421$, $Opa1^{Cd4-cre}$ T_H1: $n = 615$, $Opa1^{Cd4-cre}$ T_H2: $n = 786$, $Opa1^{Cd4-cre}$ T_H17: $n = 554$ and $Opa1^{Cd4-cre}$ T_reg: $n = 433$ cristae, and 3 biological replicates. Data are shown as individual measurements and geometric mean (red bar). **e**, Left, oxygen consumption rate (OCR) on addition of oligomycin (oligo), fluoro-carbonyl cyanide phenylhydrazone

(FCCP) and rotenone plus antimycin A (Rot + AA) ($n = 7$ injections, 3 biological replicates). Right, baseline OCR, ATP-coupled respiration and maximal respiration ($n = 3$ independent experiments). **f**, Basal glycolytic rate and total glycolytic capacity ($n = 4$ biological replicates), measured by extracellular acidification rate (ECAR). **g**, Cells expressing IFNγ, IL-17A, GATA3 and FOXP3 following restimulation ($n = 4$ biological replicates). The percentage of cells in each quadrant is indicated. **h**, Heat map of cytokine expression in the supernatant of indicated cells types, shown as log_2 fold change (FC) ($n = 3$ biological replicates). **i**, TBET and ROR-γt expression ($n = 4$ biological replicates). gMFI, geometric mean fluorescence intensity. Representative plots and graphs summarize results of at least two independent experiments except where noted otherwise. Data in **b,c,e–g,i** are mean ± s.e.m. Two-sided Tukey's test (**b,d**), Dunnett's test (**c**), Šidák's test (**e,f**) or unpaired two-tailed t-test (**g,i**). Exact P-values are indicated.

mitochondrial membrane remodelling (Fig. 1b and Extended Data Fig. 1c–e). OPA1 regulates cristae morphology and inner mitochondrial membrane fusion[6,12]. OPA1 isoforms affect pro-fusion activity[13,14], with long isoforms associated with tighter, fused mitochondrial membrane. Accumulation of long and short OPA1 isoforms (l-OPA1 and s-OPA1, respectively) varied across cell subsets (Fig. 1b)—l-OPA1 accumulated in T_H17 cells, whereas s-OPA1 accumulated in T_H1 and T_H2 cells (Fig. 1c and Extended Data Fig. 1f).

Using distinct fluorescent reporter mice, we next analysed mitochondria ultrastructure in vivo in CD4⁺ T cells after infection or experimental autoimmune encephalomyelitis (EAE), a T_H17 cell-driven disease[15]. Interferon-γ (IFNγ)–YFP-expressing T_H1 cells infected with *Listeria monocytogenes* exhibited looser cristae than CD4⁺ T_N cells (Extended Data Fig. 1g). In mice co-expressing IL-4-GFP and FOXP3-RFP, cristae loosening was found in T_H2 cells expressing IL-4-GFP, but not in those expressing FOXP3-RFP (that is, T_reg cells) after infection with the helminth *Heligmosomoides polygyrus* (Extended Data Fig. 1g).

Looser cristae in T_H1 and T_H2 cells contrasted with tighter cristae in IL-17A-cre-eYFP-expressing T_H17 cells at the peak of EAE disease (Extended Data Fig. 1g), which exhibited a mitochondrial membrane configuration resembling CD4⁺ T_N cells.

OPA1 is needed for IL-17 production

We next crossed *Opa1*-floxed mice with *Cd4-cre* mice (generating *Opa1^{Cd4-cre}* mice) to delete OPA1 in T cells. In vitro-generated T cell subsets from these mice showed disrupted mitochondrial morphology and function upon OPA1 loss (Fig. 1d–f and Extended Data Fig. 2a–d). Whereas *Opa1^{Cd4-cre}* T_H17 cells expressed less interleukin-17A (IL-17A), *Opa1^{Cd4-cre}* T_H1 cells did not show decreased expression of IFNγ and tumour necrosis factor (TNF) and *Opa1^{Cd4-cre}* T_H2 cells did not show decreased expression of IL-4, IL-5 and IL-13 (Fig. 1g,h). Lineage-specifying transcription factor expression remained intact across subsets regardless of genotype (Fig. 1g,i).

OPA1 loss decreased cell proliferation, which was not associated with reduced viability, but rather defective cell cycle progression, as more cells expressed the proliferation marker Ki67 in the G2 and M phase (Extended Data Fig. 2e–g). Reduced IL-17A expression in $Opa1^{Cd4-cre}$ was independent of cell division, early activation marker expression, or T cell receptor (TCR) or IL-6 signal strength (Extended Data Fig. 2h–j). Thus, OPA1 sustains cytokine production in T_H17 cells in vitro, but not early differentiation events associated with transcription factor expression.

Loss of mitofusin 1 (MFN1) or dynamin-related protein 1 (DRP1)—which mediate OMM fusion and fission, respectively—did not affect T cell function (Extended Data Fig. 3a–e), whereas loss of MFN2—which controls OMM fusion, interorganelle tethering and calcium signalling—altered immunometabolic function across subsets (Extended Data Fig. 3a–e). Thus, OMM remodelling per se does not sustain T_H17 effector function, and fusion-independent roles of MFN2 probably affect mitochondrial function to control T_H17 effector function in a similar manner to OPA1. Notably, DRP1 deletion in $Opa1^{Cd4-cre}$ cells re-established OMM configuration and respiration but not IL-17A expression (Extended Data Fig. 3f–i), indicating that OPA1 supports T_H17 effector function independently of its role in respiration.

OPA1 sustains T_H17 cells in vivo

T_H17 cells maintain gut homeostasis and protect against pathogens, as well as participate in inflammatory diseases[15]. These different functional states—non-pathogenic (npT_H17) and pathogenic (pT_H17)—exhibit distinct cytokine expression and metabolism[16]. OPA1 deletion disrupted cristae, cytokine expression, proliferation and cell cycle progression, but not viability or transcription factor expression in $CD4^+ T_N$ cells cultured under npT_H17 (with TGFβ and IL-6) or pT_H17 (with IL-23, IL-6 and IL-1β) conditions (Extended Data Fig. 4a–f), illustrating that both cellular states rely on OPA1.

T_H17 cells respond to segmented filamentous bacteria in the mesenteric lymph nodes (MLNs) and then migrate to the gut lamina propria for effector function[17,18]. Small intestine lamina propria cells isolated from reporter mice in which OPA1 is deleted in IL-17A-expressing cells ($Il17a$-cre × $Rosa26R$-$eYFP^{19}$ × $Opa1^{fl}$, ($Opa1^{Il17a-cre}$)) showed similar expression of markers of tissue-resident T_H17 cells (CD44, CD25, PD-1 and CCR6) and Ki67 to cells from control mice ($Il17a$-cre × $Rosa26R$-$eYFP$) (Fig. 2a,b and Extended Data Fig. 4g–h). $Opa1^{Il17a-cre}$ mice had a decreased frequency of T_H17 cells in the lamina propria, but not in the Peyer's patches or MLNs (Fig. 2c and Extended Data Fig. 4i), suggesting that OPA1 maintains small intestine lamina propria T_H17 cells.

T_H17 cells expand in the small intestine lamina propria upon treatment with anti-CD3 antibody[20]. In this model, $Opa1^{Il17a-cre}$ mice had reduced numbers of T_H17 cells in the lamina propria compared with control mice (Fig. 2d and Extended Data Fig. 4j). $Opa1^{Il17a-cre}$ T_H17 cells expressed less IL-17A and RORγt (Fig. 2e and Extended Data Fig. 4k) but similar levels of activation, migration and proliferation markers compared with control T_H17 cells (Extended Data Fig. 4l,m), supporting a requirement for OPA1 for effector function and expansion. Following immunization with myelin oligodendrocyte glycoprotein, $Opa1^{Il17a-cre}$ mice were protected from EAE (Fig. 2f and Extended Data Fig. 4n), exhibiting decreased T cell and neutrophil infiltration to the spinal cord (Fig. 2g and Extended Data Fig. 4o,p). $Opa1^{Il17a-cre}$ T_H17 cells showed defective IL-17A production (Fig. 2h), with similar expression of transcription factors (Fig. 2i), chemokine receptors CCR6 and CXCR3 and the mTOR targets pS6 and p4E-BP1 (Extended Data Fig. 4q,r). Moreover, levels of Ki67 and active caspase-3 showed that $Opa1^{Il-17a-cre}$ T_H17 cells proliferated normally, but were less viable than control T_H17 cells (Fig. 2j,k). Thus, OPA1 is required for the maintenance of tissue-resident intestinal and pathogenic T_H17 cells.

T_H17 cells need OPA1 independent of energetics

Cells depend on respiration in low-glucose conditions[21]. We explored whether differences in T cell metabolism drive the selective reliance on
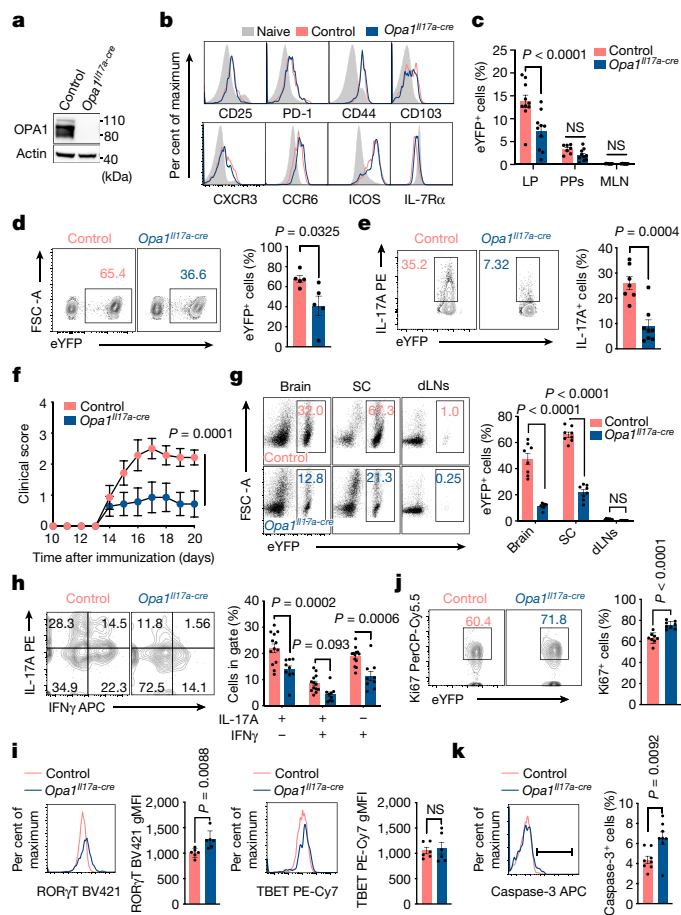

Fig. 2 | OPA1 deficiency in IL-17A-expressing cells ameliorates T_H17-mediated autoimmune pathogenesis. a, Immunoblot of $CD4^+TCRβ^+$ cells expressing enhanced yellow fluorescent protein (eYFP) (T_H17 cells) isolated from control and $Opa1^{Il17a-cre}$ reporter mice. Actin is used as a loading control. **b**, Surface markers on $CD4^+TCRβ^+eYFP^+$ cells and $CD4^+ T_N$ cells ($CD4^+CD44^{low}CD62L^{high}$) from small intestine lamina propria. **c**, Frequency of live $CD4^+TCRβ^+eYFP^+$ cells in the small intestine lamina propria (LP) (control: $n = 10$, $Opa1^{Il17a-cre}$: $n = 10$ mice), Peyer's patches (PPs) (control: $n = 7$, $Opa1^{Il17a-cre}$: $n = 10$ mice) and MLN (control: $n = 8$, $Opa1^{Il17a-cre}$: $n = 10$ mice), 2 independent experiments. **d,e**, Mice were injected with anti-CD3 antibody every 48 h for 100 h. Frequency of $CD4^+TCRβ^+eYFP^+$ cells ($n = 5$ mice) (**d**) and IL-17A expression in restimulated $CD4^+TCRβ^+eYFP^+$ cells (**e**) (control: $n = 7$, $Opa1^{Il17a-cre}$: $n = 8$ mice, 2 independent experiments). **f**, Mice were immunized with myelin oligodendrocyte glycoprotein (MOG) peptide and monitored for clinical disease score ($n = 7$ mice per group). **g**, Frequency of $CD4^+TCRβ^+eYFP^+$ cells from brain, spinal cord (SC) and draining lymph nodes (dLNs) 20 days after immunization ($n = 8$ mice per genotype, 2 independent experiments). **h**, Expression of IL-17A and IFNγ in brain $CD4^+TCRβ^+eYFP^+$ cells (control: $n = 13$, $Opa1^{Il17a-cre}$: $n = 9$ mice, 2 independent experiments). **i–k**, Expression of RORγt and TBET (**i**; $n = 6$ mice per genotype), Ki67 (**j**) and active caspase-3 (**k**) ($n = 8$ mice per genotype, 2 independent experiments) in $CD4^+TCRβ^+eYFP^+$ cells from brain (**i**) and spinal cord (**j,k**). Representative plots and graphs summarize results of at least two independent experiments, except where noted otherwise. Data are mean ± s.e.m. Two-sided Šidák's test (**c,f–h**) or unpaired two-tailed t-test (**d,e,i–k**). Exact P-values are indicated.

respiration and OPA1. The robust glycolytic and energetic metabolism in T_H1 and T_H2 cells contrasted with that in T_H17 and T_{reg} cells, which had more quiescent and oxidative metabolism with reduced glucose and leucine uptake and mTORC1 activity (Extended Data Fig. 5a,b). T_H17 cells exhibited lower rates of protein and RNA synthesis and increased dependence on mitochondrial metabolism for protein translation[22] (Extended Data Fig. 5c,d). To lower metabolic activity in an energetic

Article

cell type, we cultured T_H1 cells at different glucose concentrations (Extended Data Fig. 5e). At low glucose concentration, control T_H1 cells expressed IFNγ, whereas IFNγ expression was severely impaired in OPA1-deficient T_H1 cells (Extended Data Fig. 5f). We next explored whether low metabolic activity in T_H17 cells makes them dependent on OPA1 for IL-17 expression. It is known that pT_H17 and npT_H17 cells have distinct metabolic profiles[23]. pT_H17 cells had higher metabolic activity than npT_H17 cells, with increased oxidative metabolism and protein and RNA synthesis, as well as reduced dependence on mitochondrial metabolism for protein translation (Extended Data Fig. 5g–i), but still required OPA1 for IL-17 expression (Extended Data Fig. 4b,d). Thus, whereas low metabolic activity confers OPA1 dependence, T_H17 cells require OPA1 for cytokine expression independent of their metabolic state.

OPA1 affects glutamine flux and 2-HG

$Opa1^{Cd4-cre}$ T_H17 cells exhibited transcriptional and proteomic changes associated with immune function, infection, immune-mediated diseases and metabolic pathways compared with control T_H17 cells (Fig. 3a and Extended Data Fig. 6a–c). Proteomic analysis revealed reduced expression of electron transport chain (ETC) complex subunits and increased expression of serine and glycine biosynthesis enzymes in these cells (Extended Data Fig. 6c), suggesting mitochondrial dysfunction and a stress response[24,25], and metabolomics showed accumulation of TCA cycle metabolites, with the α-ketoglutarate (α-KG)-derived metabolite 2-hydroxyglutarate (2-HG) being highly upregulated (Fig. 3b,c). Increased NADH/NAD+ and reduced aspartate (Fig. 3d)—the production of which depends on a functional ETC[26,27]—further indicated disrupted oxidative phosphorylation (OXPHOS) and TCA cycle metabolism in OPA1-deficient cells. Similar ATP and AMP levels, glucose flux to fatty acids and lipid accumulation across genotypes (Extended Data Fig. 6d–g), ruled out a bioenergetic failure[28] or decreased de novo fatty acid synthesis[29] underlying impaired IL-17A expression in OPA1-deficient cells.

$Opa1^{Cd4-cre}$ T_H17 cells exhibited lower glucose flux to glycolysis, TCA cycle and other associated pathways (Fig. 3e,f). Notably, glucose flux to serine biosynthesis[30] decreased upon OPA1 loss (Fig. 3g), although it did not impede intracellular serine and glycine levels, which were increased in $Opa1^{Cd4-cre}$ T_H17 cells (Fig. 3h). OPA1-deficient T_H17 cells robustly incorporated glutamine-derived carbons into glutamate, TCA cycle intermediates and 2-HG (Fig. 3f,i). To test the effect of accumulated TCA cycle metabolites and 2-HG on IL-17 production, we cultured CD4+ T_N cells in T_H17 conditions with cell-permeable forms of these metabolites. IL-17A production and cell numbers were markedly reduced by 2-HG (Fig. 3j), independently of transcription factor expression or 2-HG enantiomer configuration (L-2-HG or D-2-HG) (Fig. 3k). Thus, OPA1 deletion increases glutamine oxidation and 2-HG generation, which negatively affects IL-17A expression.

Altered metabolism affects chromatin

Epigenetic and transcriptional programmes are regulated by 2-HG[5]; 2-HG inhibits α-KG-dependent DNA and histone dioxygenases and demethylases, increasing histone and/or DNA methylation[7]. Permissive (H3K4me3, H3K27ac and H3K9ac) and repressive (H3K9me3 and H3K27me3) histone modifications and global DNA methylation, increased in $Opa1^{Cd4-cre}$ T_H17 cells (Fig. 3l), suggesting altered chromatin organization. The DNA and histone methyltransferase inhibitors 5-azacytidine (5-Aza) and UNC1999 (UNC), but not histone acetyltransferase inhibitors, restored IL-17A expression (Extended Data Fig. 7a), indicating that DNA and histone methylation changes caused altered IL-17A activity. Using assay for transposase-accessible chromatin with high throughput sequencing (ATAC–seq) we found that OPA1 deficiency altered chromatin accessibility in regions with recognition motifs for

T cell differentiation, transcription factors and stress response elements (Extended Data Fig. 7b–d). Pathway annotation analysis showed that these regions were involved in transcriptional regulation, signalling and T cell responses, including IL-17A, IL-6 and LAG3 (Fig. 3m and Extended Data Fig. 7e). These data suggest that mitochondrial disturbances (that is, OPA1 deficiency) augment glutamine oxidation with 2-HG accumulation, which affects T_H17 effector function by altering the chromatin accessibility of immune response genes.

LKB1 responds to OPA deficiency

To investigate signals coordinating the cellular response to OPA1 deficiency in T_H17 cells, we performed Ingenuity pathway analysis and identified LKB1 (encoded by Stk11) as the top potential upstream regulator (Fig. 4a). LKB1 has roles in mitochondrial function, metabolism and energy homeostasis[31–34]. Notably, LKB1 also coordinates serine metabolism and DNA methylation with cancer transformation[35]. LKB1 activity, as determined by Ser428 phosphorylation[36], was increased in $Opa1^{Cd4-cre}$ T_H17 cells (Fig. 4b). Increased LKB1 phosphorylation occurred 48 h after activation in T_H17 conditions, but was absent in T_H1 and T_H2 conditions, and only appeared at later times in T_{reg} cells (Extended Data Fig. 8a,b), demonstrating differential LKB1 signalling in $Opa1^{Cd4-cre}$ T_H17 cells.

LKB1 deletion restores IL-17

Deletion of LKB1 in OPA1-deficient T_H17 cells restored IL-17A expression (Fig. 4c and Extended Data Fig. 8c,d). LKB1 deletion did not affect early activation markers, but reduced RORγt expression, proliferation and cell cycle progression[36,37] (Extended Data Fig. 8e–h). Heterozygous LKB1 loss in $Opa1^{Il17a-cre}$ mice ($Opa1Stk11het^{Il17a-cre}$) mildly restored disease and T cell infiltration compared with $Opa1^{Il17a-cre}$ mice (Extended Data Fig. 8i,j). However, full LKB1 deletion ($Opa1Stk11^{Il17a-cre}$) restricted disease and T cell infiltration (Extended Data Fig. 8k–m), probably owing to proliferation defects caused by LKB1 loss (Extended Data Fig. 8g,h), but re-established IL-17A production (Extended Data Fig. 8n), demonstrating that LKB1 senses mitochondrial integrity in vivo to control T_H17 effector function. LKB1 deletion corrected IL-17A expression in $Opa1^{Cd4-cre}$ T_H17 cells without restoring respiration or cristae morphology defects (Fig. 4d,e), and in an AMPK- and mTOR-independent manner (Extended Data Fig. 9a–e). Remarkably, LKB1 loss preserved IL-17A expression in cells treated acutely with mitochondrial inhibitors (Fig. 4f). Overall, LKB1 signalling restrains IL-17A expression following mitochondrial disturbances, and its loss unleashes cytokine expression during mitochondrial stress.

Several kinases regulate LKB1 in response to signals such as DNA damage, NADH/NAD+ imbalance, cAMP, calcium levels or reactive oxygen species[38] (ROS). OPA1-deficient cells showed alterations in many of these signals (Extended Data Fig. 9f–i), indicating that multiple factors may converge on LKB1 during mitochondrial stress. Pharmacological inhibition of LKB1-activating kinases, or restoration of the NADH/NAD+ balance or ROS pointed to ataxia telangiectasia mutated (ATM) kinase as a driver of LKB1 signalling upon OPA1 deficiency (Extended Data Fig. 9j). Thus, T_H17 cells are sensitive to perturbed mitochondrial membrane integrity and function, and this information is relayed through LKB1 to control IL-17 expression.

The OPA1–LKB1 axis regulates TCA and 2-HG

We analysed the transcriptome of LKB1-deleted control and $Opa1^{Cd4-cre}$ T_H17 cells (Extended Data Fig. 10a). Analysis of genes differentially regulated by LKB1 revealed pathways associated with amino acid biosynthesis, cytokine–cytokine receptor interaction, cell cycle and carbon metabolism (Fig. 4g and Extended Data Fig. 10b–d), illustrating processes by which LKB1 may control IL-17A expression upon
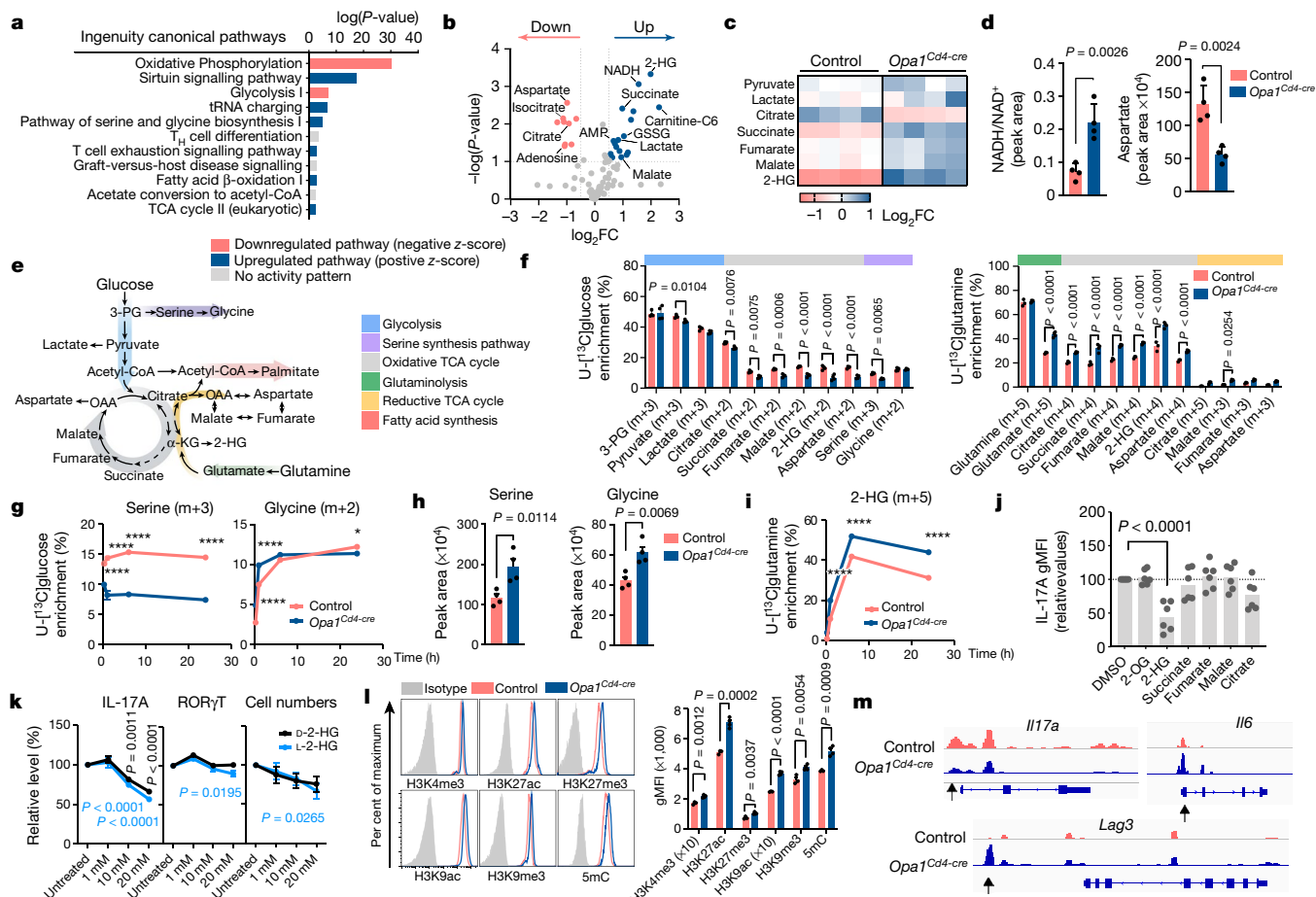
Fig. 3 | OPA1 modulates the TCA cycle and 2-HG for epigenetic control of T$_H$17 cell function. a, Ingenuity pathway analysis of differentially regulated proteins (*Opa1*$^{Cd4-cre}$ versus control T$_H$17 cells; log$_{10}$(*P*-value < 1.3, log$_2$FC > 0.58)). **b**, Volcano plot of metabolite levels determined by liquid chromatography–mass spectrometry (LC–MS) analysis. The plot shows metabolites that are increased (blue) or decreased (red) in *Opa1*$^{Cd4-cre}$ versus control T$_H$17 cells; FC > 0.5 and log$_{10}$(*P*-value) > 1. GSSG, oxidized glutathione. **c**, Heat map showing metabolite levels (log$_2$FC) in control and *Opa1*$^{Cd4-cre}$ T$_H$17 cells. **d**, Cellular NADH/NAD$^+$ (left) and aspartate (right), determined by LC–MS. **e**, Schematic of central carbon metabolism. 3-PG, 3-phosphoglycerate; OAA, oxaloacetate. **f**, Fractional labelling of metabolites in T$_H$17 cells cultured for 20 h with fully-labelled U-[^{13}C]glucose on day 3 (left, *n* = 4 biological replicates per group) or U-[^{13}C]glutamine (right, control: *n* = 3, *Opa1*$^{Cd4-cre}$: *n* = 4 biological replicates). Colours along the top of the graph correspond to the scheme in **e**. **g**, Fractional labelling of serine and glycine from U-[^{13}C]glucose. **h**, Intracellular serine and glycine levels, determined by LC–MS. **i**, Fractional labelling of 2-HG

from U-[^{13}C]glutamine. **j**, IL-17A expression in CD4$^+$ T cells cultured for 4 days in T$_H$17 conditions after overnight treatment with metabolites (*n* = 6 biological replicates, 2 independent experiments). 2-OG, 2-oxoglutarate. **k**, Cell numbers (*n* = 7 biological replicates) and cytokine and transcription factor expression (*n* = 8 biological replicates) in cells cultured for 3 days in T$_H$17 conditions with D-2-HG (black) or L-2-HG (blue) for the last 48 h, 2 independent experiments. **l**, Acetylation and methylation status of histone H3 lysine 4 (H3K4), lysine 9 (H3K9) and lysine 27 (H3K27) and DNA methylation. 5mC, 5-methylcytosine. **m**, Accessible chromatin regions as indicated by ATAC–seq. Representative plots and graphs summarize results of at least two independent experiments. Arrows indicate differentially accessible chromatin regions. **a,g,i**, *n* = 3 biological replicates. **b–d,h,l**, *n* = 4 biological replicates. Data in **d,f–l** are mean ± s.e.m. Two-sided Šidák's test (**f,g,i,k**), Dunnett's test (**j**) or unpaired two-tailed *t*-test (**d,h,l**). Exact *P*-values are indicated. *P < 0.05, ****P < 0.0001.

OPA1 deficiency. Among them, LKB1 deletion reduced the expression of serine biosynthesis enzymes (Fig. 4h), including PHGDH, the first enzyme in serine biosynthesis, which converts the glycolytic intermediate 3-phosphoglycerate to phosphohydroxypyruvate. We measured glucose flux into serine[30] in control and *Opa1*$^{Cd4-cre}$ T$_H$17 cells in which LKB1 was deleted. OPA1-deficient cells diverted less glucose to serine—as previously observed (Fig. 3g)—and LKB1 deletion reduced this further (Fig. 4i). Although serine biosynthesis was decreased, *Opa1*$^{Cd4-cre}$ T$_H$17 cells had high intracellular serine compared with controls, and these levels increased upon acute LKB1 deletion (Extended Data Fig. 10e), probably reflecting differences in extracellular serine uptake and/or catabolism. The disparity between the expression of serine biosynthesis pathway enzymes and the activity of the pathway led us question how this might affect the cellular response to OPA1 deficiency.

LKB1 coordinates TCA, NADH and 2-HG

In hypoxic or acidic conditions, NADH-dependent dehydrogenases, including PHGDH and lactate dehydrogenase (LDHA) engage in promiscuous activity and catalyse the NADH-dependent reduction of α-KG to L-2-HG and D-2-HG in addition to their primary enzymatic reactions[39–41]. We speculated that PHGDH, which was expressed in OPA1-deficient T cells, but not fully engaged in serine biosynthesis (Fig. 4h,i), produced 2-HG. We therefore pharmacologically targeted PHGDH and other dehydrogenases, including LDHA and TCA cycle enzymes that produce 2-HG, isocitrate dehydrogenase 1 and 2 (IDH1/2) and malate dehydrogenase 1 and 2[7] (MDH1/2) (Extended Data Fig. 10f). Out of these interventions, only PHGDH inhibition restored IL-17A in OPA1-deficient T$_H$17 cells (Fig. 4j and Extended Data Fig. 10f). Furthermore, PHGDH inhibition reduced glutamine flux to 2-HG in OPA1-deficient cells (Fig. 4k),
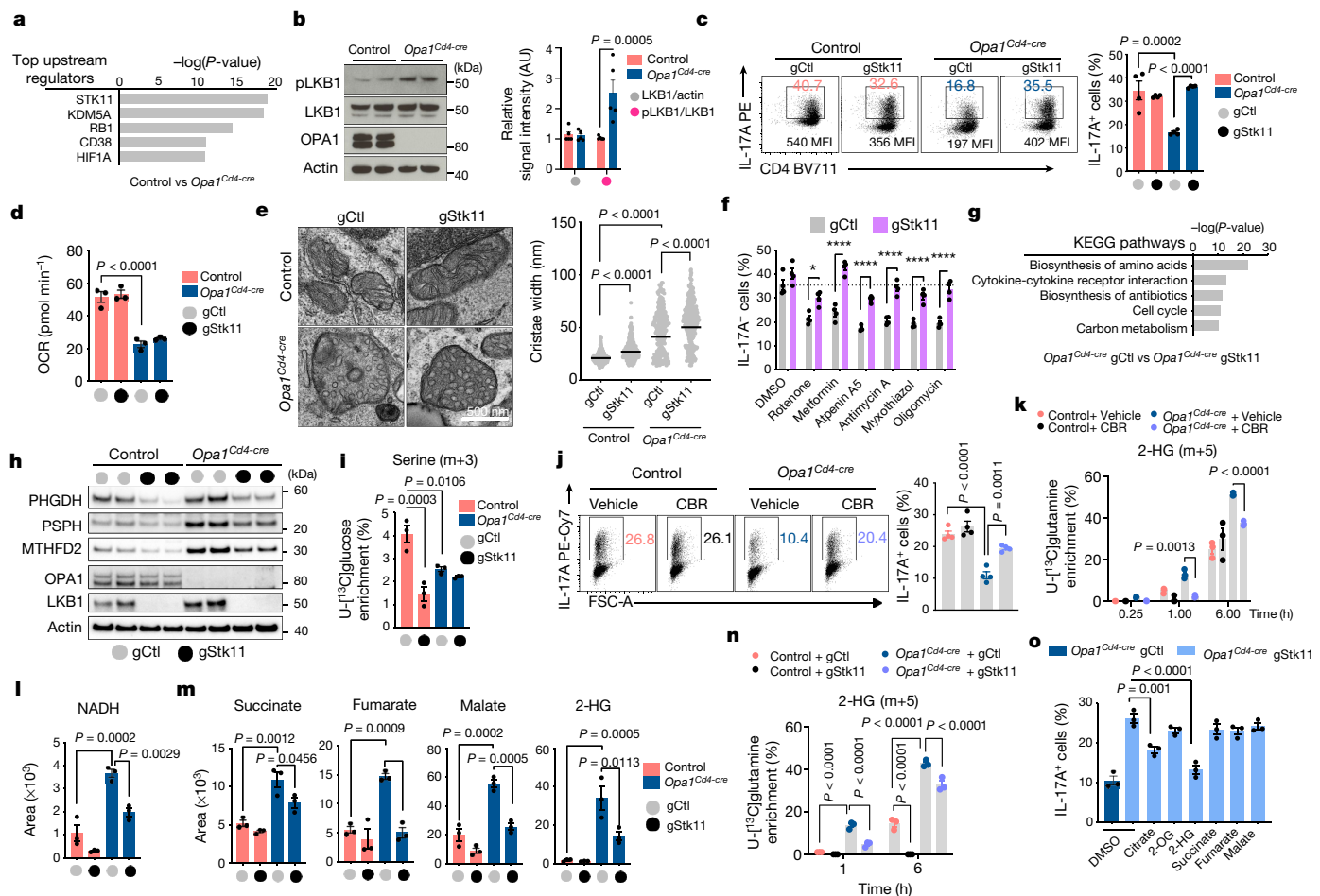
Fig. 4 | LKB1 couples TCA cycle and de novo serine metabolism for 2-HG production. a, Top upstream regulators of differentially regulated proteins ($Opa1^{Cd4\text{-}cre}$ versus control T_H17 cells; $\log_{10}$(P-value < 1.3, $\log_2$FC > 0.58, Ingenuity pathway analysis)). **b**, Immunoblot (left) and quantification (right) of LKB1 phosphorylation and expression ($n = 5$ biological replicates, 2 independent experiments). Actin is used as a sample processing control. **c**, IL-17A expression in T cells transfected with Cas9 and indicated guide RNAs (gRNAs). gCtl, control guide RNA; gStk11, $Stk11$-targeting guide RNA. **d**, Basal OCR. **e**, Electron microscopy image (left) and width of mitochondrial cristae (right) (control gCtl: $n = 214$; control gStk11: $n = 271$, $Opa1^{Cd4\text{-}cre}$ gCtl: $n = 236$; $Opa1^{Cd4\text{-}cre}$ gStk11: $n = 257$ cristae, 3 biological replicates). Data are shown as individual measurements and geometric mean (black bar). **f**, IL-17A expression in T cells transfected with Cas9 and indicated gRNAs, cultured in T_H17 conditions for four days and treated overnight as indicated. **g**, Kyoto Encyclopedia of Genes and Genomes (KEGG) pathway annotation of differentially expressed genes

($Opa1^{Cd4\text{-}cre}$ gStk11 versus $Opa1^{Cd4\text{-}cre}$ gCtl, $P < 0.001$, $\log_2$FC > 1). **h**, Immunoblot in T_H17 cells transfected with Cas9 and indicated gRNAs. Two replicate transfections shown. **i**, Detection of serine (m+3) in cells cultured for 6 h with U-[^{13}C]glucose. **j**, IL-17A expression in cells treated for 20 h with CBR-5884 on day 2. **k**, Detection of 2-HG (m+5) fractional labelling from U-[^{13}C]glutamine. **l,m**, Intracellular NADH (**l**), succinate, fumarate, malate and 2-HG (**m**) detection by LC–MS. **n**, 2-HG (m+5) in cells cultured with U-[^{13}C]glutamine. **o**, IL-17A expression in $Opa1^{Cd4\text{-}cre}$ T cells transfected with Cas9 and indicated gRNAs, cultured in T_H17 conditions for four days and treated overnight as indicated. Representative plots and graphs summarize results of at least two independent experiments, except where noted otherwise. Data **a,d,e,g,i,k–o**: $n = 3$ biological replicates per group; **c,f,j**: $n = 4$ biological replicates per group. Data in **b–d,f,i–o** are mean ± s.e.m. Two-sided Šidák's test (**b,f**), Tukey's test (**c–e,i–n**) or Dunnett's test (**o**). Exact P-values are indicated.

indicating that PHGDH contributes to 2-HG production and decreases IL-17A expression.

ETC inhibition, genetic mitochondrial deficiencies and hypoxia impair respiration and cause NADH accumulation through mitochondrial serine catabolism and—specifically—methylenetetrahydrofolate dehydrogenase[42] (MTHFD2). We tested whether LKB1 loss, which reduced serine biosynthesis enzymes (Fig. 4h), would similarly re-establish NADH levels in OPA1-deficient cells. Indeed, LKB1 deletion restored NADH in $Opa1^{Cd4\text{-}cre}$ cells to control levels (Fig. 4l) as well as TCA cycle metabolites and 2-HG (Fig. 4m). Notably, LKB1 loss decreased the exacerbated glutamine carbon allocation to TCA metabolites and 2-HG in $Opa1^{Cd4\text{-}cre}$ cells (Fig. 4n and Extended Data Fig. 10g). Consistent with LKB1 restraining IL-17A expression by regulating TCA cycle metabolites and 2-HG, single metabolite treatment—and most significantly 2-HG—dampened IL-17A expression

in LKB1-deficient $Opa1^{Cd4\text{-}cre}$ T_H17 cells (Fig. 4o). Overall, our results indicate that LKB1, by coordinating glutamine oxidation and PHGDH activity, generates 2-HG that modulates the cell's epigenetic state and restrains IL-17A expression.

Discussion

Here we show that mitochondrial disturbances in OPA1-deficient cells trigger a response that increases the expression of serine biosynthesis enzymes and 2-HG production. Loose cristae in OPA1-deficient cells alter the electron flow through the disorganized ETC, leading to increased NADH/NAD$^+$ and TCA cycle inhibition[43], as it requires NAD$^+$ for enzymatic reactions[5]. Our findings indicate that NADH accumulation pushes PHGDH to generate 2-HG from α-KG[39]—reinforcing glutamine oxidation in the TCA cycle as cells need to replenish α-KG. We

show that LKB1 responds to OPA1 deficiency by controlling glutamine oxidation and TCA cycle metabolism. LKB1 signalling exacerbates mitochondrial deficiencies in OPA1-deficient T_H17 cells, and its deletion is sufficient to restore intracellular metabolites and IL-17A expression. Although it is linked to glutamine oxidation[44], how LKB1 regulates glutamine usage remains unclear, but during mitochondrial stress it could affect redox shuttles, glutamine intake and hydrolysis or serine biosynthesis enzyme expression. Nevertheless, our findings are consistent with a role for glutamine metabolism in T_H17 cells[45]. We do not exclude the possibility that TCA cycle metabolites and 2-HG—which can regulate gene expression by epigenetic and transcriptional remodelling or protein function via posttranslational modifications[46]—may control T_H17 effector function upon mitochondrial stress through other mechanisms.

During immune responses, T cells must adapt to fluctuating environments to meet their metabolic demands and tune effector function[47]. How mitochondrial membrane rearrangements modulate cell metabolism and immune function in inflammatory environments in vivo is currently unknown. However, our data suggest that an LKB1–mitochondrial axis sustains T cell metabolic adaptations to distinct inflammatory and tissue conditions, and illustrate metabolic and mitochondrial vulnerabilities in T_H17 cells that might be therapeutically exploited to control autoimmune disease.

Online content

Any methods, additional references, Nature Research reporting summaries, source data, extended data, supplementary information, acknowledgements, peer review information; details of author contributions and competing interests; and statements of data and code availability are available at https://doi.org/10.1038/s41586-022-05264-1.

1. Buck, M. D., O'Sullivan, D. & Pearce, E. L. T cell metabolism drives immunity. *J. Exp. Med.* **212**, 1345–1360 (2015).
2. Bailis, W. et al. Distinct modes of mitochondrial metabolism uncouple T cell differentiation and function. *Nature* **571**, 403–407 (2019).
3. Xu, T. et al. Metabolic control of T_H17 and induced T_{reg} cell balance by an epigenetic mechanism. *Nature* **548**, 228–233 (2017).
4. Giacomello, M., Pyakurel, A., Glytsou, C. & Scorrano, L. The cell biology of mitochondrial membrane dynamics. *Nat. Rev. Mol. Cell Biol.* **21**, 204–224 (2020).
5. Martinez-Reyes, I. & Chandel, N. S. Mitochondrial TCA cycle metabolites control physiology and disease. *Nat. Commun.* **11**, 102 (2020).
6. Cogliati, S. et al. Mitochondrial cristae shape determines respiratory chain supercomplexes assembly and respiratory efficiency. *Cell* **155**, 160–171 (2013).
7. Ye, D., Guan, K. L. & Xiong, Y. Metabolism, activity, and targeting of D- and L-2-hydroxyglutarates. *Trends Cancer* **4**, 151–165 (2018).
8. Chan, D. C. Mitochondrial dynamics and its involvement in disease. *Annu. Rev. Pathol.* **15**, 235–259 (2020).
9. Youle, R. J. & van der Bliek, A. M. Mitochondrial fission, fusion, and stress. *Science* **337**, 1062–1065 (2012).
10. Matilainen, O., Quiros, P. M. & Auwerx, J. Mitochondria and epigenetics—crosstalk in homeostasis and stress. *Trends Cell Biol.* **27**, 453–463 (2017).
11. Herkenne, S. et al. Developmental and tumor angiogenesis requires the mitochondria-shaping protein Opa1. *Cell Metab.* **31**, 987–1003.e1008 (2020).
12. Song, Z., Chen, H., Fiket, M., Alexander, C. & Chan, D. C. OPA1 processing controls mitochondrial fusion and is regulated by mRNA splicing, membrane potential, and Yme1L. *J. Cell Biol.* **178**, 749–755 (2007).
13. Ishihara, N., Fujita, Y., Oka, T. & Mihara, K. Regulation of mitochondrial morphology through proteolytic cleavage of OPA1. *EMBO J.* **25**, 2966–2977 (2006).
14. MacVicar, T. & Langer, T. OPA1 processing in cell death and disease—the long and short of it. *J. Cell Sci.* **129**, 2297–2306 (2016).
15. Korn, T., Bettelli, E., Oukka, M. & Kuchroo, V. K. IL-17 and Th17 Cells. *Annu. Rev. Immunol.* **27**, 485–517 (2009).
16. Wagner, A. et al. Metabolic modeling of single Th17 cells reveals regulators of autoimmunity. *Cell* **184**, 4168–4185.e4121 (2021).
17. Ivanov, I. I. et al. Induction of intestinal Th17 cells by segmented filamentous bacteria. *Cell* **139**, 485–498 (2009).
18. Sano, T. et al. An IL-23R/IL-22 circuit regulates epithelial serum amyloid A to promote local effector Th17 responses. *Cell* **163**, 381–393 (2015).
19. Hirota, K. et al. Fate mapping of IL-17-producing T cells in inflammatory responses. *Nat. Immunol.* **12**, 255–263 (2011).
20. Esplugues, E. et al. Control of T_H17 cells occurs in the small intestine. *Nature* **475**, 514–518 (2011).
21. Birsoy, K. et al. Metabolic determinants of cancer cell sensitivity to glucose limitation and biguanides. *Nature* **508**, 108–112 (2014).
22. Arguello, R. J. et al. SCENITH: a flow cytometry-based method to functionally profile energy metabolism with single-cell resolution. *Cell Metab.* **32**, 1063–1075.e1067 (2020).
23. Gaublomme, J. T. et al. Single-cell genomics unveils critical regulators of Th17 cell pathogenicity. *Cell* **163**, 1400–1412 (2015).
24. Bao, X. R. et al. Mitochondrial dysfunction remodels one-carbon metabolism in human cells. *eLife* **5**, e10575 (2016).
25. Nikkanen, J. et al. Mitochondrial DNA replication defects disturb cellular dNTP pools and remodel one-carbon metabolism. *Cell Metab.* **23**, 635–648 (2016).
26. Birsoy, K. et al. An essential role of the mitochondrial electron transport chain in cell proliferation is to enable aspartate synthesis. *Cell* **162**, 540–551 (2015).
27. Sullivan, L. B. et al. Supporting aspartate biosynthesis is an essential function of respiration in proliferating cells. *Cell* **162**, 552–563 (2015).
28. Wu, L. et al. Niche-selective inhibition of pathogenic Th17 cells by targeting metabolic redundancy. *Cell* **182**, 641–654.e620 (2020).
29. Berod, L. et al. De novo fatty acid synthesis controls the fate between regulatory T and T helper 17 cells. *Nat. Med.* **20**, 1327–1333 (2014).
30. Locasale, J. W. et al. Phosphoglycerate dehydrogenase diverts glycolytic flux and contributes to oncogenesis. *Nat. Genet.* **43**, 869–874 (2011).
31. Blagih, J., Krawczyk, C. M. & Jones, R. G. LKB1 and AMPK: central regulators of lymphocyte metabolism and function. *Immunol Rev* **249**, 59–71 (2012).
32. MacIver, N. J. et al. The liver kinase B1 is a central regulator of T cell development, activation, and metabolism. *J. Immunol.* **187**, 4187–4198 (2011).
33. He, N. et al. Metabolic control of regulatory T cell (T_{reg}) survival and function by Lkb1. *Proc. Natl Acad. Sci. USA* **114**, 12542–12547 (2017).
34. Yang, K. et al. Homeostatic control of metabolic and functional fitness of T_{reg} cells by LKB1 signalling. *Nature* **548**, 602–606 (2017).
35. Kottakis, F. et al. LKB1 loss links serine metabolism to DNA methylation and tumorigenesis. *Nature* **539**, 390–395 (2016).
36. Shackelford, D. B. & Shaw, R. J. The LKB1–AMPK pathway: metabolism and growth control in tumour suppression. *Nat. Rev. Cancer* **9**, 563–575 (2009).
37. Tiainen, M., Ylikorkala, A. & Makela, T. P. Growth suppression by Lkb1 is mediated by a G_1 cell cycle arrest. *Proc. Natl Acad. Sci. USA* **96**, 9248–9251 (1999).
38. Kullmann, L. & Krahn, M. P. Controlling the master-upstream regulation of the tumor suppressor LKB1. *Oncogene* **37**, 3045–3057 (2018).
39. Fan, J. et al. Human phosphoglycerate dehydrogenase produces the oncometabolite D-2-hydroxyglutarate. *ACS Chem. Biol.* **10**, 510–516 (2015).
40. Intlekofer, A. M. et al. Hypoxia induces production of L-2-hydroxyglutarate. *Cell Metab.* **22**, 304–311 (2015).
41. Intlekofer, A. M. et al. L-2-Hydroxyglutarate production arises from noncanonical enzyme function at acidic pH. *Nat. Chem. Biol.* **13**, 494–500 (2017).
42. Yang, L. et al. Serine catabolism feeds NADH when respiration is impaired. *Cell Metab.* **31**, 809–821.e806 (2020).
43. Buck, M. D. et al. Mitochondrial dynamics controls T cell fate through metabolic programming. *Cell* **166**, 63–76 (2016).
44. Faubert, B. et al. Loss of the tumor suppressor LKB1 promotes metabolic reprogramming of cancer cells via HIF-1α. *Proc. Natl Acad. Sci. USA* **111**, 2554–2559 (2014).
45. Johnson, M. O. et al. Distinct regulation of Th17 and Th1 cell differentiation by glutaminase-dependent metabolism. *Cell* **175**, 1780–1795.e1719 (2018).
46. Baksh, S. C. & Finley, L. W. S. Metabolic coordination of cell fate by α-ketoglutarate-dependent dioxygenases. *Trends Cell Biol.* **31**, 24–36 (2021).
47. Buck, M. D., Sowell, R. T., Kaech, S. M. & Pearce, E. L. Metabolic instruction of immunity. *Cell* **169**, 570–586 (2017).

Article

Methods

Animal models

C57BL/6J (000664), PhAM (018397), Cd4-cre (022071), Il17a-cre (016879), Rosa26-eYFP (006148), Great (IFNγ eYFP reporter, 017581)[48], 4Get (IL-4 eGFP reporter, 004190)[49], FIR (FOXP3-RFP reporter, 008374)[50] and conditional floxed Stk11 (Stk11[fl], 014143) mice were purchased from The Jackson Laboratory. Opa1 and Drp1 conditional floxed mice were obtained from H. Sesaki. Mfn1 and Mfn2 conditional floxed mice were obtained from D. C. Chan. Conditional floxed mice were crossed with Cd4-cre to generate Opa1[Cd4-cre], Mfn1[Cd4-cre], Mfn2[Cd4-cre], Drp1[Cd4-cre] and Stk11[Cd4-cre] mice. For conditional deletion of OPA1 or LKB1 in IL-17A-expressing cells, Il17a reporter animals (Il17a-cre × Rosa26e-YFP, which harbour a loxP-site-flanked STOP cassette followed by the eYFP-encoding sequence inserted into the Rosa26 locus[19]) were crossed with Opa1^{fl/fl} mice (Il17-cre^{+/-} Rosa26e-YFP^{+/-} Opa1^{fl/fl} (Opa1[Il17a-cre])) or Stk11^{fl/fl} mice (IL17Cre^{+/-} R26eYFP^{+/-} Stk11^{fl/fl} (Stk11[Il17Cre])). For conditional deletion of OPA1 and LKB1, Cd4-cre or Il17a reporter mice were crossed with Opa1^{fl/fl} and Stk11^{fl/fl} mice (Cd4-cre^{+/-} Opa1^{fl/fl} Stk11^{fl/fl}, Opa1Stk11[Cd4-cre]; Il17Cre^{+/-} Rosa26-eYFP^{+/-} Opa1^{fl/fl} Stk11^{fl/+}, Opa1Stk11het[Il17-cre] and Il17-cre^{+/-} Rosa26-eYFP^{+/-} Opa1^{fl/fl} Stk11^{fl/fl} (Opa1Stk11[Il17-cre])). Age- and sex-matched Il17a reporter animals (Il17-cre^{+/-} Rosa26-eYFP^{+/-} (control)) were used as controls. All mice were used at 8–12 weeks of age unless otherwise noted. All mice required for this study were bred in specific-pathogen-free conditions in the animal facility of the Max Planck Institute for Immunobiology and Epigenetics (Freiburg, Germany), and all corresponding animal protocols were approved by the animal care committee of the Regierungspraesidium Freiburg. All cells used in this study were collected from male and female mice at 8–12 weeks of age.

T cell assays

CD4^{+} T_N cells were isolated from cell suspensions from spleen and peripheral lymph nodes from mice from the indicated genotypes. Pooled spleen and lymph node single cell suspensions were incubated with biotinylated antibodies against mouse CD44, CD25, CD8, IgM, B220, CD19, Gr-1, MHC-II, F4/80, CD11c, CD11b and DX5 (Biolegend), followed by negative selection using magnetic beads (Stem cell Technology). Approximately 0.3×10^6 CD4^{+} T_N cells were plated into 48-well-plates coated with 5 µg ml^{−1} anti-mouse CD3 (clone 17A2, BioXcell), 2 µg ml^{−1} soluble anti-mouse CD28 (clone 37.51, BioXcell) in RPMI 1640 (Gibco) supplemented with 10% fetal calf serum (Gibco), 1% (v/v) penicillin–streptomycin (Invitrogen), 55 µM β-mercaptoethanol (Sigma), 1 mM sodium pyruvate, 2 mM glutamine and 5 mM Hepes. For T_H1 conditions, culture was supplemented with IL-12 (10 ng ml^{−1}) and anti-mouse IL-4 (4 µg ml^{−1}, clone 11B11, BioXcell). For T_H2 conditions, IL-4 (10 ng ml^{−1}) and anti-mouse IFNγ (4 µg ml^{−1}, clone XMG1.2, BioXcell) were added. For T_H17 conditions, TGFβ (5 ng ml^{−1}), IL-6 (10 ng ml^{−1}), IL-1β (10 ng ml^{−1}), anti-mouse IFNγ (10 µg ml^{−1}) and anti-mouse IL-4 (10 µg ml^{−1}) were included in cell cultures. For regulatory T cell conditions, TGFβ (10 ng ml^{−1}), anti-mouse IFNγ (4 µg ml^{−1}) and anti-mouse IL-4 (4 µg ml^{−1}) were added. Where specificied, cells were polarized towards non-pathogenic (np) and pathogenic (p) T_H17 cell conditions as follows. For npT_H17 conditions, TGFβ (5 ng ml^{−1}), IL-6 (10 ng ml^{−1}), anti-mouse IFNγ (10 µg ml^{−1}) and anti-mouse IL-4 (10 µg ml^{−1}) were included in cell cultures. For pT_H17 conditions, IL-6 (20 ng ml^{−1}), IL-1β (20 ng ml^{−1}), IL-23 (20 ng ml^{−1}), anti-mouse IFNγ (10 µg ml^{−1}) and anti-mouse IL-4 (10 µg ml^{−1}) were included in cell cultures. Human IL-2 (10 ng ml^{−1}) was added to all cultures except in T_H17 conditions. All cytokines were from PrepoTech. The cells were supplemented with fresh medium at day 3 and analyses performed at day 4 unless otherwise stated.

For analysis of intracellular cytokine production and transcription factor expression, cells were collected on day 4 and restimulated 6 h with phorbol myristate acetate (50 ng ml^{−1}) (PMA) and ionomycin (1 µg ml^{−1}) in the presence of brefeldin A (Biolegend) for the last 4 h.

After restimulation, cells were stained with cell-surface marker antibodies and LIVE/DEAD Fixable dye Blue (Thermo) to exclude dead cells, fixed and permeabilized with a FOXP3/transcription factor staining kit (eBioscience), followed by staining with cytokine- and/or transcription-factor-specific antibodies. All flow cytometry analyses were performed on an LSR III flow cytometer (BD) and data were analysed with FlowJo software (BD).

For analysis of cytokines in cell culture supernatants, equal numbers of cells were collected and cultured in fresh medium containing PMA and ionomycin for 16 h on day 4. After restimulation, supernatant was collected and concentration of cytokines determined by a multiplexed assay (LEGENDplex, Biolegend), as per manufacturer instructions.

Mitochondrial ETC inhibitors were added overnight on day 3 of culture with the following doses: 1 µM rotenone (Sigma), 5 mM metformin (Sigma), 1 µM atpenin A5 (Hellobio), 1 µM antimycin A (Sigma), 1 µM myxothiazol (Sigma), 1 µM oligomycin (Sigma). AMPK inhibitor Compound C (Merk) was added at 1 mM from the initial activation (day 0) or 16 h at day 3. Cells were treated with the following TCA metabolites as indicated; 1 mM dimethyl oxoglutarate, 5 mM diethyl succinate, 100 nM diethyl fumarate, 0.25 mM octyl-2-HG, L- and D-α-hydroxyglutaric acid disodium salt, 1 mM diethyl malate, and 1 mM citrate (all from Sigma).

The following compounds were added for 48 h in cells at day 1 of culture at 10 µM unless otherwise indicated: CBR-5884 (Sigma), BAY 1436032 (MedChemExpress), LW6 (TCI Deutschland), AGI-5198 (Sigma), NHI-2 (Sigma), GSK-864 (Sigma), CPTH2 (Cayman), Anacardic acid (Cayman), A485 (Tocris), 1 µM C6464 (Sigma), Sinefungin (Abcam), 1 µM 5-aza-2′-deoxycytidine (Sigma), 1 µM UNC1999 (Abcam), KDM5-C70 (Xcess Bio), 1 µM GSK-J4 (Xcess Bio), KU-55933 (Sigma), 0.5 µM BI-D1870 (Abcam), 1 µM Ex-527 (Abcam), 1 µM sirtinol (Fischer Scientific), 1 µM PKCζ pseudosubstrate inhibitor (Cayman), 1 µM PKC ζ pseudosubstrate inhibitor, myristoylated (sc-397537, Santa Cruz Biotechnology), 1 µM PKA Inhibitor 14-22 Amide, Myristoylated (Sigma), 0.5 mM nicotinamide riboside (Cayman), 1 µM Tempol (Santa Cruz), 5 mM N-acetylcysteine (NAC) from Sigma. Cells were processed for flow cytometry and acquired with CytExpert software on a CytoFLEX (Beckman Coulter) cytometer and data analysed with FlowJo software v10.7.2. (BD).

CRISPR–Cas9 delivery

CRISPR–Cas9 deletion of LKB1, DRP1 and AMPKα1 was performed with Alt-R CRISPR–Cas9 System (IDT) and 4D-Nucleofector technology (Lonza) in freshly isolated CD4^{+} T cells. gRNA duplexes were prepared by mixing equimolar concentrations of CRISPR RNAs (crRNAs) and trans-activating crRNAs (tracrRNAs), annealing 5 min at 98 °C, mixing gRNA complexes (crRNA–tracrRNA) with Alt-R Streptococcus pyogenes Cas9 Nuclease V3 (IDT), and incubating for 20 min at room temperature to form ribonucleoprotein (RNP) complexes (crRNA–tracrRNA–Cas9). For the delivery of RNP complexes, cells were extensively washed in PBS, pelleted, and the RNP complexes and P4 Primary Cell buffer added before transferring into a nucleofection chamber. The complexes were delivered by electroporation using DS137 pulse on Amaxa 4D-Nucleofector (Lonza). Electroporated cells were recovered in T cell medium for 120 min at 37 °C before activation in T_H conditions, as described. Two gRNAs were used to target LKB1 (Mm.Cas9.STK11.1.AA: 5′-GGGCTCGTACGGCAAGGTGA-3′; Mm.Cas9.STK11.1.AC: 5′-TTGACGTTGGCCTCTCCATT-3′), DRP1 (Mm.Cas9.DNM1L.1.AA: 5′-GTTCCCACTACGACGATCTG-3′; Mm.Cas9.DNM1L.1.AB: 5′-AAATAGCTATGGTGAACCGG-3′) and AMPKα subunit 1 (Mm.Cas9.PRKAA1.1.AA: 5′-CGAGTTGACCGGACATAAAG-3′; Mm.Cas9.PRKAA1.1.AB: 5′-CCGGTGTGGATTATTGTCAC-3′), and a non-targeting gRNA (Alt-R CRISPR–Cas9 negative control crRNA) was used as control (all from IDT) at same concentration of RNP complexes between conditions.

Metabolic assays

OCR (in pmol min^{−1}) and ECAR (in mpH min^{−1}) were measured in a 96-well XF Extracellular Flux Analyzer (Seahorse Bioscience) on cells at day 4 of

activation. Cells (10^5 per well; at least 3 injections per condition) were plated in complete XF medium (non-buffered RPMI 1640 containing 25 mM glucose, 2 mM L-glutamine, and 1 mM sodium pyruvate) and spun onto poly-D-lysine-coated Seahorse 96-well plates. Cells were equilibrated for 1 h at 37 °C in the absence of CO_2 before the assay. OCR and ECAR were measured in basal conditions and in response to 1 μM oligomycin, 1.5 μM FCCP and 100 nM rotenone + 1 μM antimycin A (all from Sigma). Basal mitochondrial respiration was determined from baseline measurements. ATP-coupled respiration was determined by the subtraction of oligomycin A values from basal respiration. Maximal mitochondrial respiration was determined by subtracting the OCR after treatment with rotenone and antimycin A from the OCR measured following treatment with FCCP. For glycolysis characterization, cells were plated in complete XF medium without glucose and ECAR (in mpH min^{-1}) was measured in basal conditions and in response to 10 mM glucose (Sigma), 1 μM oligomycin and 25 mM 2-deoxyglucose (2-DG, Sigma). Basal glycolytic rate was determined by subtracting ECAR measurement following 2-DG treatment from ECAR measurements following glucose addition. Total glycolytic capacity was determined by subtracting the ECAR measured after 2-DG treatment from the ECAR measured after oligomycin treatment.

Glucose uptake was analysed by flow cytometry in CD4$^+$ T cells cultured in complete RPMI medium without glucose (Gibco) containing 100 mM 2-NBDG (Sigma) for 20 min at 37 °C.

Kynurenine uptake was analysed by flow cytometry as described[51]. CD4$^+$ T cells were stained with anti-CD4 and plated in HBSS at 37 °C in a water bath. 200 μM kynurenine (Sigma) was added to the cells and uptake was stopped after 4 min by fixing cells in 1% paraformaldehyde (PFA, Sigma) for 30 min at room temperature. The 405 nm laser and 450/50 BP filter were used for kynurenine fluorescence detection.

Protein and RNA synthesis were analysed by flow cytometry in CD4$^+$ T cells incubated 30 min at 37 °C in complete RPMI medium containing 20 μM Click-iT O-propargyl-puromycin (OPP, Thermo) or 1 mM Click-iT 5-ethynyl uridine (EU, Thermo), respectively. Incorporation of protein and RNA Click-iT analogues was detected with a standard Click-it reaction (Thermo) following manufacturer's instructions. Negative controls for protein and RNA synthesis were included in the assay by incubation of cells with 100 μg ml^{-1} cycloheximide (Sigma) 30 min or 5 μg ml^{-1} actinomycin D (Sigma) 45 min, respectively.

For the analysis of protein translation dependence on mitochondrial function and glycolysis, protein synthesis rates in vehicle-treated cells was subtracted to protein synthesis rates of cells treated with oligomycin or 2-deoxyglucose, as described[22].

Immunoblot analysis

Cells were washed with ice-cold PBS and lysed in 1× cell lysis buffer (Cell Signaling). Cleared protein lysates were denatured (LDS loading buffer, 10 min, 70 °C), and equal number of cells or equal protein amount resolved on precast 4% to 12% NuPAGE Bis-Tris protein gels (Life Technologies), and transferred onto nitrocellulose membranes (iBLOT2, Life Technologies). To resolve long and short OPA1 isoforms, equal amounts of protein lysates were run for at least 100 min in precast 8% Bis-Tris protein gels (Life Technologies), and transferred onto nitrocellulose membranes (iBLOT2, Life Technologies).

Membranes were blocked in TBS-Tween 5% milk for 1 h at room temperature and incubated overnight at 4 °C with the following antibodies (dilution; clone; catalogue number); anti-β-actin (1:5,000; 13E5; 4970S), anti-LKB1 (1:2,000; D60C5; 3047S), anti-phosphorylated LKB1 Ser428 (1:2,000; C67A3, 3482S), anti-AMPKα (1:2,000; D5A2; 5831S), anti-phosphorylated AMPKα Thr172 (1:2,000; 40H9; 2535), anti-phosphorylated ACC Ser79 (1:2,000; 3661), anti-ACC (1:2,000; C83B10; 3676), anti-DRP1(1:2,000; D6C7; 8570), anti-TOM20 (1:2,000; D8T4N; 42406) and anti-MFN2 (1:2,000; D2D10; 9482) from Cell Signaling, anti-OPA1 (1:2,000; 18/OPA1; 612606) from BD Biosciences, anti-MFN1 (1:1,000; EPR21953-74; ab221661) from Abcam, anti-tubulin

(1:4,000; DM1A; T9026) and anti-PHGDH (1:2,000; HPA021241) from Sigma, anti-PSPH (1:2,000; PA5-96863) from Thermo and anti-MTHFD2 (1:2,000; 12270-1-AP) from Proteintech.

All primary antibody incubations were followed by three TBS-Tween washes (10, 5 and 5 min, respectively) and 1 h incubation with secondary HRP-conjugated antibodies (1:10,000 for rabbit anti-mouse IgG (H+L) secondary antibody, HRP (31450) or 1:20,000 for goat anti-rabbit IgG (H+L) secondary antibody, HRP (31460)) from Thermo Fisher in TBS-Tween with 5% milk. Membranes were washed with TBS-Tween (10, 5 and 5 min, respectively) and visualized using SuperSignal West-Pico or Femto Chemiluminescent Substrate (Pierce) on Biomax MR films (Kodak) or the ChemiDoc Imaging System (Bio-Rad). Optical intensity of the signals was quantified using ImageJ software (v1.53c, NIH). Tubulin or β-actin were used as loading controls when samples were run in same gels or as sample processing controls, when run on parallel gels.

Uncropped and unprocessed scans of all blots are provided in the Source data files.

Imaging analysis of mitochondrial structure

Spinning disk confocal microscopy was performed as described[43]. For live imaging of mitochondria in cells from PhAM mice, CD4$^+$ T$_N$ cells were purified and activated as indicated for four days, transferred to glass bottom dishes (MatTek) pre-coated with poly-D-lysine (Sigma) in complete RPMI medium, and acquired using a Zeiss spinning disk confocal with an Evolve (EMCCD) camera with a 100× objective. Cells were kept in a humidified incubation chamber at 37 °C with 5% CO_2 during acquisition. For nuclei visualization, Hoechst 42 (Thermo) was added prior to acquisition. For the analysis of mitochondrial morphology in fixed cells, cells from the indicated genotypes were activated as indicated, stained with Mitotracker Deepred 30 min at 37 °C, allowed to settle for 30 min at 37 °C into poly-D-lysine-coated coverslips, fixed 10 min with 2% PFA in PBS, and mounted with Prolong antifade medium containing DAPI (Invitrogen). At least 15 fields were randomly acquired per condition and biological replicate. Confocal images were analysed using Imaris analysis software (v9.5, Bitplane).

For electron microscopy imaging 0.5–1.0 × 10^6 T cells were fixed in 2.5% glutaraldehyde in 100 mM sodium cocodylate, washed in cocodylate buffer. After dehydration samples were embedded in Eponate 12 resin (Ted Pella) and sections were cut. Images were acquired using a JOEL 1200 EX trans-mission electron microscope with an ATMP digital camera. Cristae width was measured using ImageJ software (v1.53c, NIH) and averaged over 40 independent images in 3 biologically independent samples per condition. Acquisition of electron microscopy micrographs and measurements of max cristae width displayed were performed blinded.

For electron microscopy analysis of mitochondrial structure in ex vivo T cells: great mice (which express an IRES-enhanced YFP construct after the *Ifng* stop codon that allows expression of both IFNγ and eYFP from the same mRNA and then analysis of IFNγ-expressing cells) were injected intravenously with a sublethal dose 1 × 10^4 colony-forming units (CFU) of wild-type *L. monocytogenes*. T cells were sorted by fluorescence-activated cell sorting (FACS) (CD4$^+$IFNγ-eYFP$^+$ live cells) from cell suspensions from spleen and peripheral lymph nodes obtained at day 7 post-infection and processed for electron microscopy as indicated. For *H. polygyrus* infection, mice expressing IL-4-eGFP (which express an IRES-enhanced EGFP construct between the translational stop codon and the 3′ UTR of the interleukin 4 gene, and allow the analysis of IL-4 expressing cells) and FOXP3-RFP (which express a bicistronic reporter expressing a red fluorescent protein knocked into the endogenous *Foxp3* locus, and allow the analysis of FOXP3-expressing cells) were gavaged with 200 infectious L3 stage *H. polygyrus* larvae in PBS. On day 14, MLNs were collected and CD4 T cells were FACS-sorted (CD4$^+$IL-4-eYFP$^+$ live cells, for T$_H$2 CD4 T cells and CD4$^+$FOXP3-RFP$^+$ live cells, for T$_{reg}$ cells) and processed for electron

microscopy as indicated. T_N cells were FACS-sorted from the spleen and lymph nodes from steady-state C57BL/6J mice.

Mouse EAE model

EAE was induced by immunizing mice subcutaneously with 200 μg of myelin oligodendrocyte glycoprotein peptide (MOG_{35-55}: MEVG-WYRSPFSRVVHLYRNGK) emulsified in complete Freund's adjuvant (supplemented with killed *Mycobacterium tuberculosis* strain H37RLa) and intraperitoneal injections of 200 ng pertussis toxin (Hooke Labs) at the time of immunization and 24 h later. The disease was scored daily on a scale of 0–5 as follows: 0, no overt signs of disease; 1, limp tail; 2, limp tail plus hindlimb weakness; 3, hindlimb paralysis; 4, hindlimb and forelimb paralysis; 5, moribund. At the end of experiment, the mice were euthanized for analysis of the T cells infiltrated into the brain and spinal cord. Mice that did not develop symptoms of EAE were not excluded from the analysis. When indicated, the statistical significance was determined by Student's *t*-test or one-way ANOVA (exact *P*-values are presented on each graph). Sample size is indicated on each graph. All animal work was performed in compliance with all relevant ethical regulations and approved by the animal care committee of the Regierungspraesidium Freiburg and Max Planck Institute.

Mouse CD3 model

Mice were injected intra-peritoneally every 48 h during 100 h with 50 μg anti-CD3 monoclonal antibody (2C11, BioXcell) and euthanized 4 h after the last injection. Lymphocytes from small intestine lamina propria were isolated by removing Peyer's patches from the small intestine and then cutting into 1 cm pieces. Tissue was washed in RPMI 3% FCS supplemented with 5 mM EDTA (Thermo) and 0.15 mg ml^{-1} DTT by shaking 25 min at 37 °C for removal of epithelial and intraepithelial cells, washed 4 times with RPMI containing 2 mM EDTA, digested with 0.1 mg ml^{-1} Liberase TL (Roche) and 50 μg ml^{-1} DNase I (Roche) 35 min at 37 °C, followed by separation on a Percoll (GE Healthcare) gradient.

Flow cytometry

To assess cytokine production in in vitro experiments, cells were activated for the indicated times, collected and restimulated 6 h with 50 ng ml^{-1} PMA and 1 μg ml^{-1} ionomycin in the presence of brefeldin A (Biolegend) for the last 4 h. Intracellular cytokine staining was performed using BD CytoFix/CytoPerm kit (BD Biosciences) and nuclear staining of transcription factors using the FOXP3 Permeabilisation kit (eBioscience). Cells were stained with Live/Dead viability dye (Thermo) prior to antibody staining. Cells were collected on LSR III Fortessa flow cytometers (BD Bioscience) and analysed using FlowJo (BD Biosciences) software. The following antibodies were used: anti-CD4 (A20), anti-IL17A (TC11-18H10.1), anti-IFNγ (XMG1.2) and anti-TBET (4B10) from Biolegend; anti-GATA-3 (TWAJ) from eBioscience and anti-FOXP3 (FJK-16s, R16-715) and anti-RORγt (Q31-378) from BD Biosciences.

To determine eYFP$^+$ T_H17 cells (CD4+/TCRβ+) in the small intestine lamina propria, Peyer's patches and MLNs from Il17a reporter mice, lymphocytes were cell-surface stained with anti-CD45 (30-F11), anti-CD4 (A20), anti-TCRβ (H57-597) from Biolegend and LIVE/DEAD Fixable dye Blue (Thermo) and identified as live CD45$^+$CD4$^+$TCRβ$^+$eYFP$^+$ cells. For detection of T_H17 cells (CD4$^+$TCRβ$^+$) expressing eYFP in the central nervous system of EAE mice, lymphocyte fraction from the brain and spinal cord was obtained by cutting tissues in small pieces, followed by digestion with 2.4 μg ml^{-1} collagenase II (Sigma) and 4 μg ml^{-1} DNAse I (Sigma), 45 min at 37 °C and separation on a Percoll gradient. Lymphocytes were cell-surface stained with CD45 (30-F11), CD11c (N418), CD4 (A20), anti-TCRβ (H57-597) from Biolegend and LIVE/DEAD Fixable dye Blue (Thermo) and T_H17 cells identified as live CD45$^+$CD4$^+$TCRβ$^+$eYFP$^+$. For intracellular detection of cytokines in cells from the small intestine or the central nervous system, lymphocytes were restimulated 4–5 h at 37 °C in complete RPMI with PMA (50 ng ml^{-1}, Sigma) and ionomycin (1 μg ml^{-1}, Sigma) in the presence of Brefeldin A (1 μg ml^{-1}, Sigma), cell-surface stained, fixed with 2% PFA

10 min at room temperature, and stained intracellularly with IL-17A-PE (TC11-18H10.1) using the BD CytoFix/CytoPerm kit (BD Biosciences).

Analysis of cell cycle was performed by flow cytometry in cells stained with anti-CD4 and LIVE/DEAD Fixable dye for 30 min at 4 °C, fixed with FOXP3 Permeabilisation kit (eBioscience) 60 min at room temperature and stained for 40 min with Ki67 (Biolegend). DNA content was assessed by FxCycle staining (Thermo) in the live CD4$^+$ T cell gate.

Analysis of phospho-S6 ribosomal protein (S235/236) and phospho-4E-BP1 (Thr37/46) was performed by flow cytometry in CD4 T cells stained with anti-CD4, fixed with 2% PFA, permeabilized for 1 h with 90% methanol at −20 °C and stained with anti-pS6 (D57.2.2E) and p4EB-P1 (2365B4) fluorescent conjugated antibodies from Cell Signaling Technology.

Analysis of active caspase-3 was performed by flow cytometry in cells stained with anti-CD45, anti-CD4, anti-TCRβ (Biolegend) and LIVE/DEAD Fixable dye (Thermo) for 30 min at 4 °C, fixed with BD CytoFix/CytoPerm kit (BD Biosciences) and stained for 45 min with anti-active caspase-3 antibody (1:100, clone C92-605, BD Biosciences).

Analysis of the histone methylation and acetylation marks was performed by flow cytometry in CD4$^+$ T cells fixed 60 min at room temperature with FOXP3 Permeabilisation kit (eBioscience) and stained for 90 min with fluorescently labelled antibodies against H3K4me3 (clone C42D8), H3K27ac (clone D5E4), H3K27me3 (clone C36B11), H3K9ac (clone C5B11), H3K9me3 (clone D4W1U), and rabbit monoclonal antibody IgG isotype control (DA1E) (all from Cell Signaling). Cells were gated on diploid cells with 'single' DNA content based on FxCycle staining (Thermo) in the live-cell gate.

Analysis of the DNA methylation mark 5-methylcytosine (5mC) was performed by flow cytometry in CD4$^+$ T_N cells activated in T_H17 cell culture conditions for 4 days. Cells were collected, washed in PBS and stained with anti-CD4 and LIVE/DEAD Fixable dye (Thermo) for 30 min at 4 °C, followed by 60 min fixation at room temperature with FOXP3 Permeabilisation kit (eBioscience). Cells were washed, permeabilized (0.5% Triton X-100 in PBS) 15 min at room temperature and treated with 2 N HCl 30 min at 37 °C. Neutralization was performed with 100 mM Tris-HCl pH 8.8 for 10 min, followed by extensive washes with 0.05% Tween-20 in PBS. After blocking (1% BSA and 0.05% Tween-20 in PBS) for 2 h, cells were incubated with a monoclonal antibody against 5 mC (33D3, AbD Serotec) at a final concentration of 10 μg ml^{-1} or with an isotype control antibody (mouse IgG) for 90 min at room temperature. Samples were washed in 1% BSA, 0.05% Tween-20 in PBS and incubated with the secondary antibody for 35 min at room temperature. Cells were washed and incubated with FxCycle staining (Thermo) for DNA content analysis prior to flow cytometry acquisition.

Analysis of mitochondrial membrane potential was performed by flow cytometry in cells labelled 30 min with 50 nM tetramethylrhodamine methyl ester (Thermo) in complete medium and LIVE/DEAD Fixable dye (Thermo). Cells were gated on live cells and results expressed as geometric mean fluorescence intensity.

Analysis of mitochondrial content by flow cytometry was performed in CD4$^+$ T_N cells and CD4$^+$ T_N cells activated in T_H and regulatory T cell conditions for the indicated times, staining with anti-CD4 and LIVE/DEAD Fixable dye (Thermo) for 30 min at 4 °C, followed by 60 min fixation at room temperature with FOXP3 Permeabilisation kit (eBioscience) and 60 min staining at room temperature with fluorescently labelled antibodies against TOMM20 (clone EPR15581-54), ATP5A (clone 15H4C4) and COX IV (clone EPR9442(ABC)) from Abcam and Mitofilin (clone D-3) from Santa Cruz. Cells were gated on live CD4$^+$ cells and results expressed as geometric mean fluorescence intensity relative to CD4$^+$ T_N cells.

Intracellular calcium content was determined by flow cytometry with the ratiometric calcium indicator Indo-1 (Thermo) in cells incubated with Indo-1-AM (1 μM,) 30 min at 37 °C in complete RPMI medium without FCS. Cells were washed, resuspended in complete medium and the mean fluorescence intensity of the Calcium-bound and unbound Indo-1

signal acquired on a linear scale on a LSR III Fortessa flow cytometer (BD Bioscience) equipped with 37 °C temperature-controlled tube holder. Fluorescence intensity was analysed in FlowJo (BD Biosciences) software and represented as the bound/unbound Indo-1 ratio.

Quantitative PCR analysis

Total RNA was extracted using the RNeasy mini kit (Qiagen) with an additional on-column DNase treatment using the RNAse-Free DNase set (Qiagen), and quantified with Nanodrop (Thermo Fisher). cDNA was prepared using 200-300 ng total RNA by a reverse transcription PCR (RT–PCR) using a High Capacity cDNA Reverse Transcription kit (Applied Biosystems), per manufacturer's instructions. Quantitative PCR for the assessment of *Il17a* mRNA expression was performed on cDNA using TaqMan Gene Expression Assays (Assay ID:Mm00439619_m1 IL17A, Thermo Fisher) on an Applied Biosystems 7000 sequence detection system, using iTaq Universal SYBR Green Supermix (Bio-Rad). Fold changes in expression were calculated by the ΔΔCt method, using Hprt or 18s ribosomal RNA (Assay ID: Mm03024075_m1 Gene: Hprt, Assay ID: Mm03928990_g1 18s Ribosomal RNA, Thermo Fisher) as endogenous controls for mRNA expression.

RNA-sequencing analysis

RNA was extracted using RNeasy Kit (QIAGEN) following the manufacturer's instructions with an additional on-column DNase treatment using the RNAse-Free DNase set (Qiagen). RNA was quantified using Qubit 2.0 (Thermo Fisher Scientific). Libraries were prepared using the TruSeq stranded mRNA kit (Illumina) and sequenced in a HISeq 3000 (Illumina) with a read depth of approximately 30 million aligned reads per sample by the Deep-sequencing Facility at the Max Planck Institute for Immunobiology and Epigenetics (Freiburg). Sequenced libraries were processed with deepTools[52] v_2.0, using STAR[53] v_2.7.10, for trimming and mapping, and feature Counts[54] v_2.0.3 to quantify mapped reads. Raw mapped reads were processed in R (Lucent Technologies) with DESeq2[55] v_1.36 to generate normalized read counts to visualize as heatmaps using Morpheus (Broad Institute) and determine differentially expressed genes with greater than 2-fold change and lower than 0.05 adjusted *P*-value. Gene ontology analysis was performed with DAVID[56] (v_2016 and v_2021) and Ingenuity pathway analysis (QIAGEN).

ATAC–seq

Libraries were prepared using the Nextera DNA library Prep Kit (Illumina) adapting a published protocol[57]. In vitro-polarized T_H17 cells were washed in PBS and then lysed for 3 min in 10 mM Tris-HCl, pH 7.4,10 mM NaCl, 3 mM $MgCl_2$ and 0.1% Igepal CA-630, 0.1% Tween-20, 0.01% digitonin, 1% BSA (all from Sigma). Cold wash buffer (same as lysis buffer without Igepal and digitonin) was added to the lysate and mixed three times by inverting the tubes and immediately spun at 500*g* for 5 min, 4 °C. Supernatant was discarded and nuclei resuspended in 2.5 µl TDE1 (Nextera Tn5, 100 nM final), 0.5 µl 1% digitonin (0.01% final), 0.5ul 10% Tween-20 (1% final) 16.5 µl PBS and 5 µl water and incubated for 30 min at 37 °C with gentle mixing (1,000 rpm). DNA was purified with the QIAGEN MinElute PCR Purification Kit (Thermo Fisher Scientific). PCR amplification was performed with the NEBNext High-Fidelity 2× PCR Master Mix (New England Labs) using custom Nextera PCR primers containing barcodes. Adapters were removed with AMPure XP beads according to manufacturer's protocol. Libraries were quantified with the Qubit and sequenced with a HISeq 3000 (Illumina) at the Deep-sequencing Facility at the Max Planck Institute for Immunobiology and Epigenetics (Freiburg).

Sequenced samples were trimmed with Trimmomatic[58] v_0.4, mapped using Bowtie2[59] v_2.4.5 and replicate mapped files merged with SAMtools[60] v_1.4.1. Coverage files were generated with deepTools[52] v_2.0. Open chromatin and differentially regulated chromatin regions were detected with MACS2[61] v_2.2.7.1 using a *P*-value <1 × 10^−7 and a *q*-value of less than 0.1 and differentially regulated regions identified with CSAW[62,63] v_1.30.1 using a 2-fold enrichment threshold and *P*-value lower than 0.01. Bed files were analysed with Bedtools[64] v_2.28.0, and visualized alongside coverage files on IGV v_2.4.0. Transcription factor enrichment was done with HOMER[65] v_4.11.

Metabolite extraction

Equal number of cells were pelleted, medium removed by aspiration and washed once with 500 µl PBS. Metabolome extraction was performed by the addition of 10 µl ice-cold solvent (40:40:20 acetonitrile:methanol:water) every 100,000 cells. After centrifugation for 10 min at 16,000*g* at 4 °C, clean supernatant was transferred to a clean tube, frozen on dry ice and kept at −80 °C until LC–MS analysis.

LC–MS analysis

Targeted metabolite quantification by LC–MS was carried out using an Agilent 1290 Infinity II UHPLC in line with an Agilent 6495 QQQ-MS operating in MRM mode. MRM settings were optimized separately for all compounds using pure standards. LC separation was on a Phenomenex Luna propylamine column (50 × 2 mm, 3 µm particles) using a solvent gradient of 100% buffer B (5 mM ammonium carbonate in 90% acetonitrile) to 90% buffer A (10 mM NH_4 in water). Flow rate was from 1,000 to 750 µl min^−1. Autosampler temperature was 5 °C and injection volume 2 µl. Peak areas were measured using MassHunter B.07.01 (Agilent).

GC–MS analysis

To measure [^{13}C]glucose and [^{13}C]glutamine tracing, CD4$^+$ T_N cells were cultured and activated as described followed by incubation with fresh RPMI medium containing 11 mM [^{13}C]glucose or 2 mM [^{13}C]glutamine for the indicated periods of time. Cells were collected, processed for metabolome extraction and dried by SpeedVac. Dried metabolite extracts were resuspended in pyridine and derivatized with methoxyamine (sc-263468 Santa Cruz Bio) for 60 min at 37 °C and subsequently with *N*-(*tert*-butyldimethylsilyl)-*N*-methyl-trifluoroacetamid, with 1% *tert*-butyldimethylchlorosilane (375934 Sigma-Aldrich) for 30 min at 80 °C. Isotopomer distributions were measured using a DB5-MS GC column in a 7890 GC system (Agilent Technologies) combined with a 5977 MS system (Agilent Technologies). Data processing, including correction for natural isotope abundance was performed by an in-house R script (https://gitlab.gwdg.de/joerg.buescher/ metabolomics_scripts).

Lipidomics

Lipids were extracted using a biphasic methyl *tert*-butyl ether (MTBE) extraction protocol. The same number of cells per condition were resuspended in 100 µl cold PBS in glass vials. Cold methanol (750 µl), MTBE (2 ml) and water (625 µl) were added sequentially with vortexing. Samples were centrifuged to separate phases, and the upper organic phase was dried using a Genevac EZ2 speed vac. Samples were resuspended in 2:1:1 isopropanol:acetonitrile:water prior to analysis. LC–MS was carried out using an Agilent Zorbax Eclipse Plus C18 column using an Agilent 1290 Infinity II UHPLC in line with an Agilent 6495 Triple Quad QQQ-MS. Lipids were identified by fragmentation and retention time, and quantified using MassHunter B.07.01 (Agilent).

Proteomics

Sample preparation. Protein sample preparation was carried out using 5 × 10^6 cells using an iST 8X kit (PreOmics), according to the manufacturer's recommendation. All samples used for data-dependent acquisition (DDA) and data-independent acquisition (DIA) analyses were spiked with index retention time (iRT) kit peptides (Biognosys), according to the manufacturer's instructions.

Construction of DIA spectral library. Spectral libraries were generated by Spectronaut version 10.0 using MaxQuant results as an input[66]. Seventyshotgun (DDA) runs (using 2 or 3 biological replicates

Article

from each biological conditions) were acquired using a Q Exactive Plus instrument, and data were searched using MaxQuant (version 1.6.1.0). The spectral library was constructed using an FDR cut-off of 1% and a minimum and maximum of 3 and 6 fragment ions, respectively, and protein grouping was performed according to MaxQuant search results.

Mass spectrometric acquisition. The general nanoLC–MS setup was similar to that previously described[66], with minor modifications. A Q Exactive Plus mass spectrometer (Thermo Fisher) and an Easy nanoLC-1200 (Thermo Fisher) were used for both DDA and DIA experiments. For the chromatographic separation of peptides, 4 µg peptide digest was analysed at 50 °C (controlled by Sonation column oven) on a 50-cm in-house-packed fused-silica emitter microcolumn (75 µm inner diameter × 360 µm outer diameter SilicaTip PicoTip; New Objective) packed with 1.9-µm reverse-phase ReproSilPur C18-AQ beads (Dr Maisch). Peptides were separated by a 4-h linear gradient of 5–80% (80% acetonitrile, 0.1% formic acid) at a constant flow rate of 300 nl min^{-1}.

Data analysis. The MS2-based label-free quantification was carried out by analysing DIA raw data using Biognosys Spectronaut (version 10.0) software using default parameters as previously described[66], with minor modifications. In brief, the decoy method was set to 'mutated', data extraction and extraction window were set to 'dynamic' with correction factor 1, identification was set to 'normal distribution P-value estimator' with q-value cut-off of 0.1, and the profiling strategy was set to 'iRT profiling' with q-value cut-off of 0.01. Ultimately, protein quantity was set to 'average precursor quantity' and smallest quantitative unit was set to 'precursor ion' (summed fragment ions). For statistical testing and identification of deregulated proteins in all approaches, a two-sample Student's t-test was used to identify differentially expressed proteins filtered to 1% FDR.

Statistical analysis

Statistical analysis was performed using Prism 9 software (GraphPad) and Microsoft Excel (v16.46). Data are expressed as mean ± s.e.m. (standard error of the mean), unless otherwise indicated. Comparisons for two groups were calculated using unpaired two-tailed Student's t-tests (for two groups meeting the normal distribution criteria, according to the Shapiro–Wilk normality test). Comparisons of more than two groups and grouped data were calculated using one-way or two-way ANOVA, and corrected for multiple comparisons between groups or to a reference group using Tukey's, Šidák's or Dunnett's tests. Exact P-values and details of statistical testing can be found in the Figure legends and in the Source data file. Unless otherwise specified, n represents the number of individual biological replicates and is represented in graphs as one dot per sample. Flow cytometry plots are representative of at least three replicates. Immunoblots are representative of at least two independent experiments. Confocal and electron microscopy images are representative of at least three independent biological replicates. No statistical method was used to predetermine sample size, but a minimum of three samples were used per experimental group and condition. Experiments were not randomized.

Reporting summary

Further information on research design is available in the Nature Research Reporting Summary linked to this article.

Data availability

RNA-sequencing and ATAC–seq data have been deposited in the Gene Expression Omnibus (GEO) as the superseries GSE207603. This superseries contains RNA-sequencing datasets with accession numbers GSE156742 and GSE207601 and a single ATAC–seq dataset with accession

number GSE207602. The mass spectrometry proteomics data have been deposited to the ProteomeXchange Consortium via the PRIDE partner repository, with the dataset identifier PXD036162. Source data are provided with this paper.

Code availability

LC–MS and GC–MS metabolomics data were analysed using R code developed in-house, which is publicly available at https://gitlab.gwdg.de/joerg.buescher/metabolomics_scripts.

48. Reinhardt, R. L., Liang, H. E. & Locksley, R. M. Cytokine-secreting follicular T cells shape the antibody repertoire. *Nat. Immunol.* **10**, 385–393 (2009).
49. Mohrs, K., Wakil, A. E., Killeen, N., Locksley, R. M. & Mohrs, M. A two-step process for cytokine production revealed by IL-4 dual-reporter mice. *Immunity* **23**, 419–429 (2005).
50. Wan, Y. Y. & Flavell, R. A. Identifying Foxp3-expressing suppressor T cells with a bicistronic reporter. *Proc. Natl Acad. Sci. USA* **102**, 5126–5131 (2005).
51. Sinclair, L. V., Neyens, D., Ramsay, G., Taylor, P. M. & Cantrell, D. A. Single cell analysis of kynurenine and system L amino acid transport in T cells. *Nat. Commun.* **9**, 1981 (2018).
52. Ramirez, F. et al. deepTools2: a next generation web server for deep-sequencing data analysis. *Nucleic Acids Res.* **44**, W160–W165 (2016).
53. Dobin, A. et al. STAR: ultrafast universal RNA-seq aligner. *Bioinformatics* **29**, 15–21 (2013).
54. Liao, Y., Smyth, G. K. & Shi, W. featureCounts: an efficient general purpose program for assigning sequence reads to genomic features. *Bioinformatics* **30**, 923–930 (2014).
55. Love, M. I., Huber, W. & Anders, S. Moderated estimation of fold change and dispersion for RNA-seq data with DESeq2. *Genome Biol.* **15**, 550 (2014).
56. Huang da, W., Sherman, B. T. & Lempicki, R. A. Systematic and integrative analysis of large gene lists using DAVID bioinformatics resources. *Nat. Protoc.* **4**, 44–57 (2009).
57. Buenrostro, J. D., Wu, B., Chang, H. Y. & Greenleaf, W. J. ATAC–seq: a method for assaying chromatin accessibility genome-wide. *Curr. Protoc. Mol. Biol.* **109**, 21.29.21–21.29.29 (2015).
58. Bolger, A. M., Lohse, M. & Usadel, B. Trimmomatic: a flexible trimmer for Illumina sequence data. *Bioinformatics* **30**, 2114–2120 (2014).
59. Langmead, B. & Salzberg, S. L. Fast gapped-read alignment with Bowtie 2. *Nat. Methods* **9**, 357–359 (2012).
60. Li, H. et al. The Sequence Alignment/Map format and SAMtools. *Bioinformatics* **25**, 2078–2079 (2009).
61. Zhang, Y. et al. Model-based analysis of ChIP-Seq (MACS). *Genome Biol.* **9**, R137 (2008).
62. Lun, A. T. & Smyth, G. K. De novo detection of differentially bound regions for ChIP-seq data using peaks and windows: controlling error rates correctly. *Nucleic Acids Res.* **42**, e95 (2014).
63. Lun, A. T. & Smyth, G. K. csaw: a Bioconductor package for differential binding analysis of ChIP-seq data using sliding windows. *Nucleic Acids Res.* **44**, e45 (2016).
64. Quinlan, A. R. & Hall, I. M. BEDTools: a flexible suite of utilities for comparing genomic features. *Bioinformatics* **26**, 841–842 (2010).
65. Heinz, S. et al. Simple combinations of lineage-determining transcription factors prime cis-regulatory elements required for macrophage and B cell identities. *Mol. Cell* **38**, 576–589 (2010).
66. Musa, Y. R., Boller, S., Puchalska, M., Grosschedl, R. & Mittler, G. Comprehensive proteomic investigation of Ebf1 heterozygosity in pro-B lymphocytes utlizing data independent acquisition. *J. Proteome Res.* **17**, 76–85 (2018).

Author contributions F.B., K.P., D.J.P., M.V., C.S.F., L.J.F., A.Q., J.E.-H., M.A.S., K.M.G., A.M.K., B.K., M.F., M.M., G.C., M.C., K.J.D., H.S.,T.J., J.M.B., H.S., D.O., E.J.P. and E.L.P. designed and/or performed experiments. F.B., K.P., D.J.P., C.S.F., L.J.F., M.V., A.Q., J.E.-H., M.A.S., K.M.G., A.M.K., M.F., M.M., G.C., M.C., K.J.D., T.J., J.M.B., D.O., E.J.P. and E.L.P. analysed data. D.E.S. and N.R. performed all bioinformatics analysis. Y.M. and G.M. performed proteomics analysis. F.B. and E.L.P. designed the study and wrote the manuscript. All authors edited and approved the manuscript.

a

Mito sphericity (a.u.)

P <0.0001
P <0.0001   *P* <0.0001
P <0.0001

N   Th1   Th2   Th17   Treg

b

Naive   Th1   Th2   Th17   Treg

500 nm   500 nm   500 nm   500 nm   500 nm

100 nm   100 nm   100 nm   100 nm   100 nm

Cristae width (nm)

P <0.0001   *P* <0.0001
P <0.0001
P =0.0212

N   Th1   Th2   Th17   Treg

c

Cell size   Mitochondrial content

Naive
Th1
Th2
Th17
Treg

FSC-A → TOMM20 AF647 → ATP5A AF488 → Mitofillin AF564 → COXIV AF405

% of max

Relative gMFI

P <0.0001   *P* <0.0001
P <0.0001

Naive   Th1   Th2   Th17   Treg

COXIV
Mitofillin
ATP5A
TOMM20

d

N Th1 Th2 Th17 Treg

OPA1 — 80 KDa
MFN1 — 80 KDa
MFN2 — 80 KDa
DRP1 — 80 KDa
TOMM20 — 20 KDa
ACTIN — 40 KDa

e

Signal intensity (au)

ns   *ns*   *ns*   *ns*

OPA1   MFN2   MFN1   DRP1

Naive
Th1
Th2
Th17
Treg

f

Th1   Th2   Th17   Treg
N 1 2 3 4 1 2 3 4   1 2 3 4   1 2 3 4   Time (days)

L-OPA1 — 110 KDa
S-OPA1 — 80 KDa
MFN2 — 80 KDa
MFN1 — 80 KDa
DRP1 — 80 KDa
TOMM20 — 20 KDa
TUB — 50 KDa

Th1   Th17
Th2   Treg

Signal intensity (au)

OPA1   MFN2   MFN1   DRP1   TOMM20

P =0.0176
P =0.0021
P =0.0002

N 1 2 3 4   Time (days)

g

Naive   Th1   Th2   Th17   Treg
CD62h/CD44l/CD4+   IFNγ-YFP+/CD4+   IL-4-GFP+/CD4+   IL17^aCre eYFP/CD4+   Foxp3-RFP+/CD4+

100 nm

Cristae width (nm)

P =0.0318
P =0.0275
*P* =0.0001

N   Th1   Th2   Th17   Treg

Extended Data Fig. 1 | See next page for caption.

Article

Extended Data Fig. 1 | Mitochondrial membrane remodeling in CD4⁺ T_N cells under T-helper (Th) and regulatory (Treg) conditions *in vitro* and *in vivo*.
a) Mitochondrial sphericity in live cell spinning disk microscopy images in CD4⁺ T_N cells (PhAM mice) cultured in Th and Treg conditions (T_N: $n = 1673$, Th1: $n = 8406$, Th2: $n = 5485$, Th17: $n = 7672$ and Treg: $n = 4824$ segmented objects (mitochondria), 2 independent experiments. Violin plot shows median with quartiles. **b**) EM images (*left*) and cristae width (*right)* in T_N cells cultured in Th and Treg conditions (T_N: $n = 362$, Th1: $n = 479$, Th2: $n = 369$, Th17: $n = 319$, and Treg: $n = 294$ cristae, 3 biological replicates). (**c**) Intracellular expression in T_N, Th and Treg cells ($n = 4$ biological replicates). Representative graph summarize results of two independent experiments. **d**) Immunoblot of CD4⁺ T_N, Th and Treg cells, day 4, representative experiment out of two. ACTIN: sample processing control (**e**) Quantification of protein levels from immunoblots as in Fig. 1b ($n = 4$ biological replicates, 2 independent experiments). **f**) Immunoblot of proteins that control mitochondrial dynamics in CD4⁺ T_N cells cultured for the indicated times in Th and Treg conditions. TUBULIN: sample processing control. *Right*, protein levels ($n = 4$ biological replicates, 2 independent experiments). **g**) EM images (*left*) and cristae width (*right*) in CD4⁺ T_N and effector T cells from reporter mice subjected to immune challenges (naive: $n = 410$, Th1: $n = 262$, Th2: $n = 675$, Th17: $n = 461$ and Treg: $n = 402$ cristae, 3 mice per condition). Data **b**, **g** are geometric mean, **c** mean and **e**, **f** means ± s.e.m. Two-sided Tukey's test (**b**) or Dunnett's test (**a**, **c**, **e**, **f**, **g**). Exact *P* values are indicated.
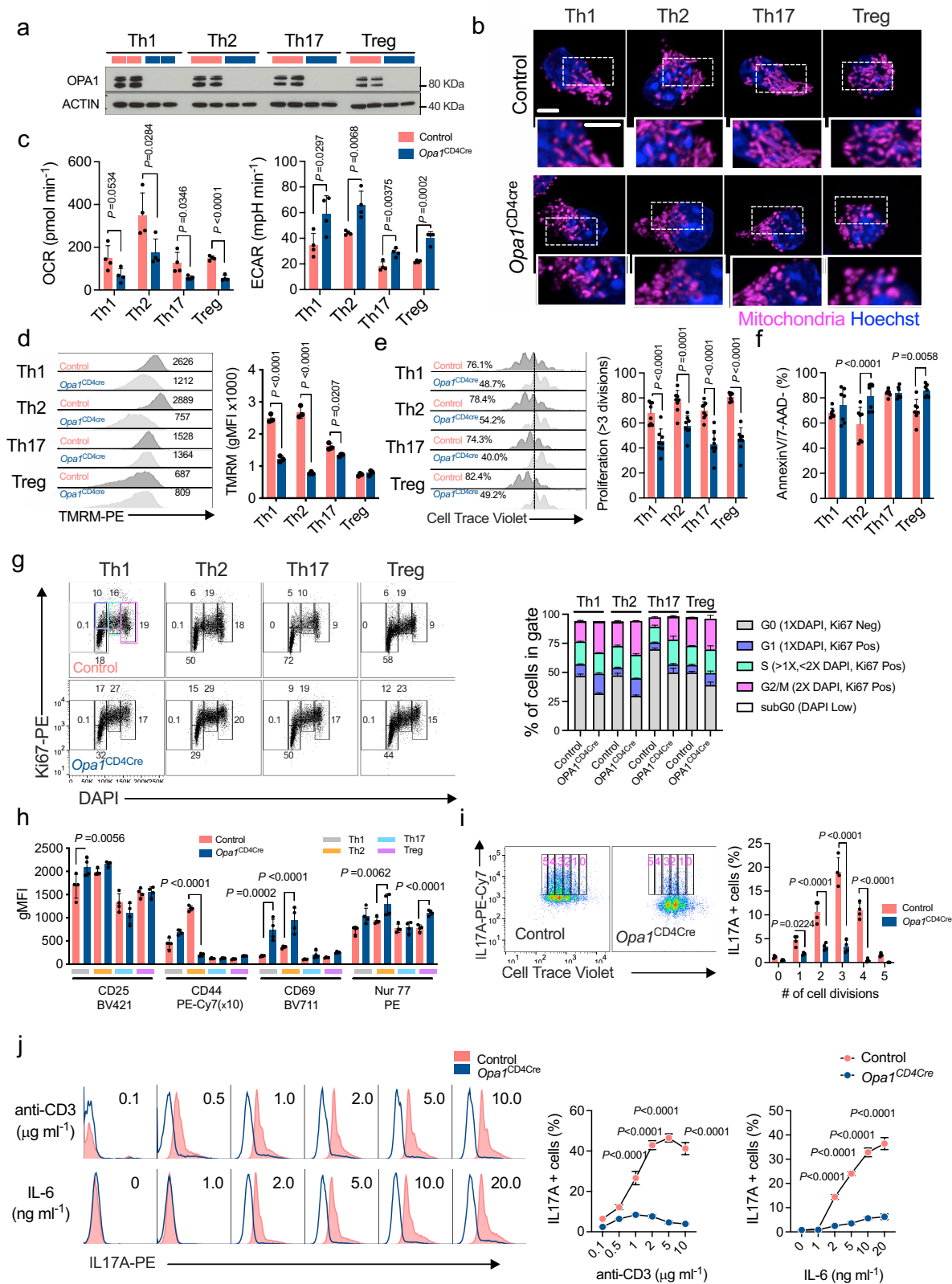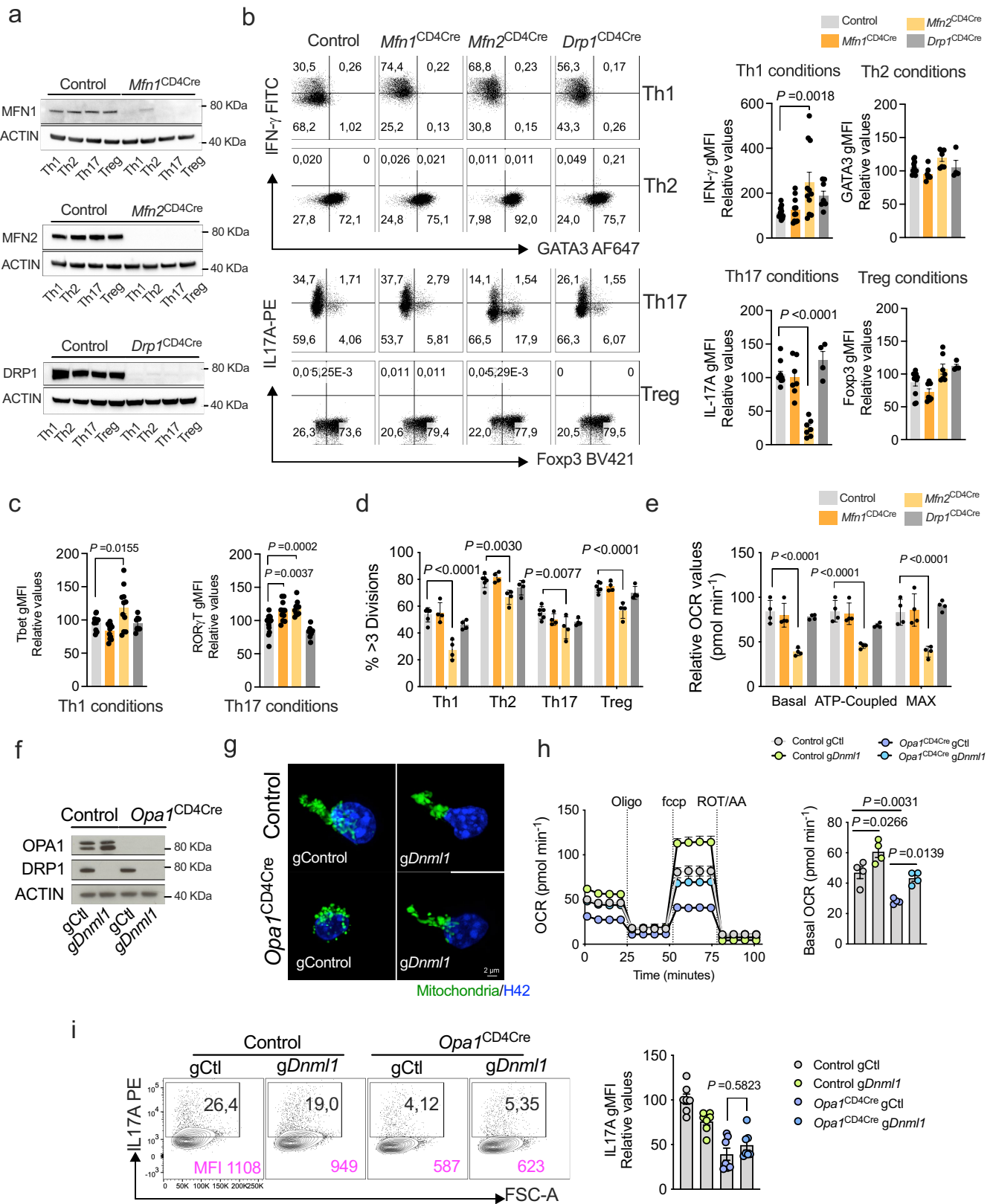
Article

Extended Data Fig. 2 | Mitochondrial dysfunction and proliferation defects in *Opa1*^{CD4Cre} T cells. CD4$^+$ T$_N$ cells from control and *Opa1*^{CD4Cre} mice were cultured 4 days in Th and Treg conditions. **a)** Immunoblot for OPA1 at the end of the culture (2 biological replicates per condition shown). ACTIN: loading control. **b)** Spinning disk microscopy images from mitochondria (MitoTracker Deep Red, purple) and nuclei (Hoechst, blue). Scale bar: 2 μm. Representative images from 3 biological replicates. **c)** Baseline OCR (*left*) and ECAR (*right*) (*n* = 4 biological replicates). **d)** Mitochondrial membrane potential determined by Tetramethylrhodamine methyl ester (TMRM) (*n* = 3 biological replicates) **e)** Cell proliferation, day 3 (*n* = 8 biological replicates, 2 independent experiments). **f)** Cell viability determined by 7-aminoactinomycin D (7-AAD) and annexin-V staining, day 4 (*n* = 7 biological replicates, 2 independent experiments). **g)** Cell-cycle analysis determined by Ki-67 and DAPI staining (*n* = 3 biological replicates). **h)** Surface expression of CD25, CD44 and CD69, and intracellular expression of Nur77 in CD4$^+$ T$_N$ cells from control and *Opa1*^{CD4Cre} mice cultured 3 days in Th and Treg conditions (*n* = 4 biological replicates). **i)** IL-17A expression and proliferation in control and *Opa1*^{CD4Cre} Th17 cells, day 3. Graph shows IL-17A expression per each cell division state gated on live CD4$^+$ T cells (*n* = 4 biological replicates). **j)** IL-17A expression in CD4$^+$ T$_N$ cells cultured in Th17 conditions with increasing concentration of plate bound anti-CD3 or IL-6 for three days and restimulated (*n* = 4 biological replicates). Representative plots and a graph summarizing the results of at least two independent experiments are shown, except where noted otherwise. Data are means ± s.e.m. Two-sided Šidák's test (**d**, **e**, **f**, **h**, **i**, **j**) or unpaired two-tailed *t*-test (**c**). Exact *P* values are indicated.
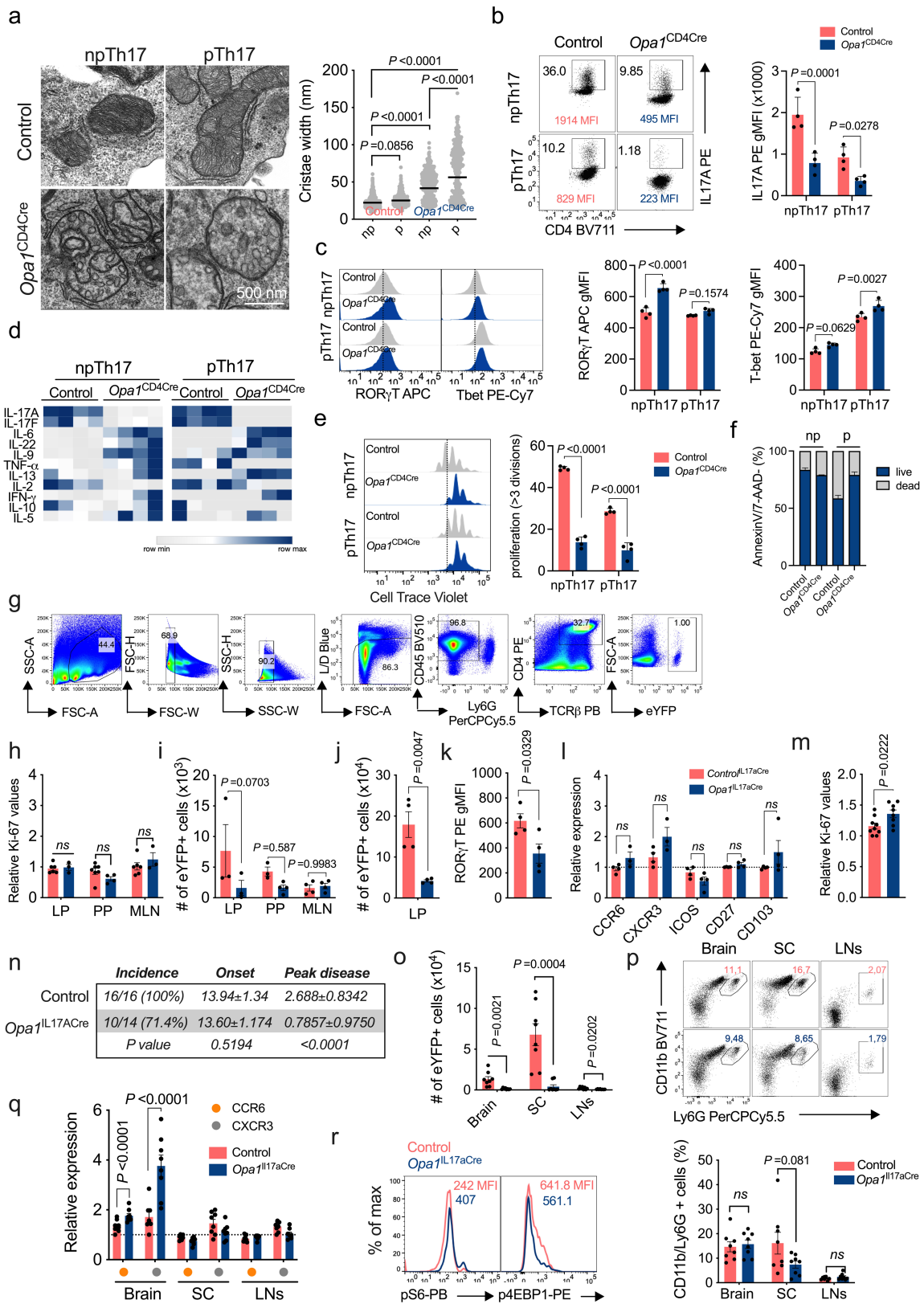
Extended Data Fig. 3 | See next page for caption.

Article

Extended Data Fig. 3 | Role of inner and outer MM remodeling in IL-17A production. *Mfn1*, *Mfn2* or *Dnml1* floxed mice were crossed with CD4Cre mice (*Mfn1*^CD4Cre, *Mfn2*^CD4Cre and *Drp1*^CD4Cre). **a**, **b**, **c**, **d**, **e**, CD4$^+$ T$_N$ cells across genotypes were cultured in Th and Treg conditions. **a**) Immunoblot of MFN1, MFN2 and DRP1 in a representative experiment out of two. ACTIN: loading control. **b**) Cytokine and TF expression in Th- and Treg-reestimulated cells across genotypes (Th1 conditions: Control n =15; Mfn1, Mfn2 n =11; Drp1 n =8; Th2, Th17 and Treg conditions; Control n =11; Mfn1, Mfn2 n =7; Drp1 n =4, biological replicates). **c**) Intracellular levels of T-bet and ROR-γt (Control n =15; *Mfn1*^CD4Cre n =11; *Mfn2*^CD4Cre n =11; *Drp1*^CD4Cre n =8, biological replicates). **d**) Proliferation as determined by Cell Trace Violet dilution staining (n = 4 biological replicates, except control; n = 6). **e**) Relative baseline OCR, ATP-coupled respiration, and maximal respiration in Th17 cells across genotypes (n = 4 biological replicates per group). **f**, **g**, **h**, **i**, Control and *Opa1*^CD4Cre CD4$^+$ T$_N$ cells were transfected with Cas9 and indicated gRNAs. **f**) Immunoblot for DRP1 and OPA1. ACTIN: loading control. **g**) Representative spinning disk confocal images from mitochondria (Mitotracker Deepred, green) and nuclei (Hoechst, blue) from 3 biological and transfection replicates. **h**) OCR upon oligomycin (Oligo), fccp and rotenone + Antimycin A (ROT+AA) addition (*left*) and relative baseline OCR (*right*) (n =4 biological and transfection replicates). **i**) Intracellular IL-17A expression (n =7 biological and transfection replicates). Representative plots and a graph summarizing the results of at least two independent experiments are shown, except where noted otherwise. Data are means ± s.e.m. Two-sided Tukey's test (**b**, **c**, **d**, **e**, **h**, **i**). Exact P values are indicated.

Extended Data Fig. 4 | See next page for caption.

Article

Extended Data Fig. 4 | OPA1-requirement for IL-17A expression across cell culture and *in vivo* conditions. T_N cells cultured in Th17 non-pathogenic (np) and pathogenic (p) conditions. **a**) EM images and cristae width (Control np: $n = 528$, p: $n = 343$; $Opa1^{CD4Cre}$ np: $n = 321$, p: $n = 267$ cristae, 3 biological replicates). Graph shows geometric mean, black. (**b**) Cytokine (**c**) TF expression, **d**) supernatant cytokines, and **e**) proliferation, $n = 4$ biological replicates. **f**) Cell viability ($n = 8$, 2 independent experiments). **g**) Gating strategy to identify CD4$^+$TCRβ$^+$eYFP$^+$ (Th17) cells. **h**) Ki-67 expression in LP Th17 cells (Control: $n = 6$; $Opa1^{IL17aCre}$: $n = 3$), PP (Control: $n = 7$; $Opa1^{IL17aCre}$: $n = 4$) and MLN (Control: $n = 6$; $Opa1^{IL17aCre}$: $n = 3$), 2 independent experiments. **i**) Th17 cell numbers (LP: $n = 3$; PP; Control: $n = 3$; $Opa1^{IL17aCre}$: $n = 4$, MLN: $n = 4$). Mice were anti-CD3 immunized. **j**) LP Th17 cell numbers ($n = 4$), **k**) ROR-γT expression ($n = 4$), **l**) surface expression (CCR6, CXCR3: Control: $n = 4$; $Opa1^{IL17aCre}$: $n = 3$; ICOS, CD27, CD103: $n = 4$) and **m**) Ki-67 levels (Control: $n = 9$; $Opa1^{IL17aCre}$: $n = 8$, 2 independent experiments). Mice were MOG immunized. **n**) Disease incidence, onset and peak disease (days, control^{IL17aCre}: $n = 16$; $Opa1^{IL17aCre}$: $n = 14$, 2 independent experiments. **o**) Cell numbers ($n = 8$). **p**) Neutrophil percentage (CD45$^+$CD11b$^+$Ly6G$^+$, $n = 8$). **q**) CCR6 and CXCR3 levels ($n = 8$). **r**) Phosphorylated S6 and 4E-BP1 (CD4$^+$TCRβ$^+$eYFP$^+$ cells). Plots and graphs summarize results of at least two independent experiments, except noted otherwise. Data are means ± s.e.m. Two-sided Tukey's test (**a**) or Šidák's test (**b**, **c**, **e**, **i**, **l**, **q**) or unpaired two-tailed t-test (**h**, **j**, **k**, **m**, **o**, **p**). Exact P values are indicated.
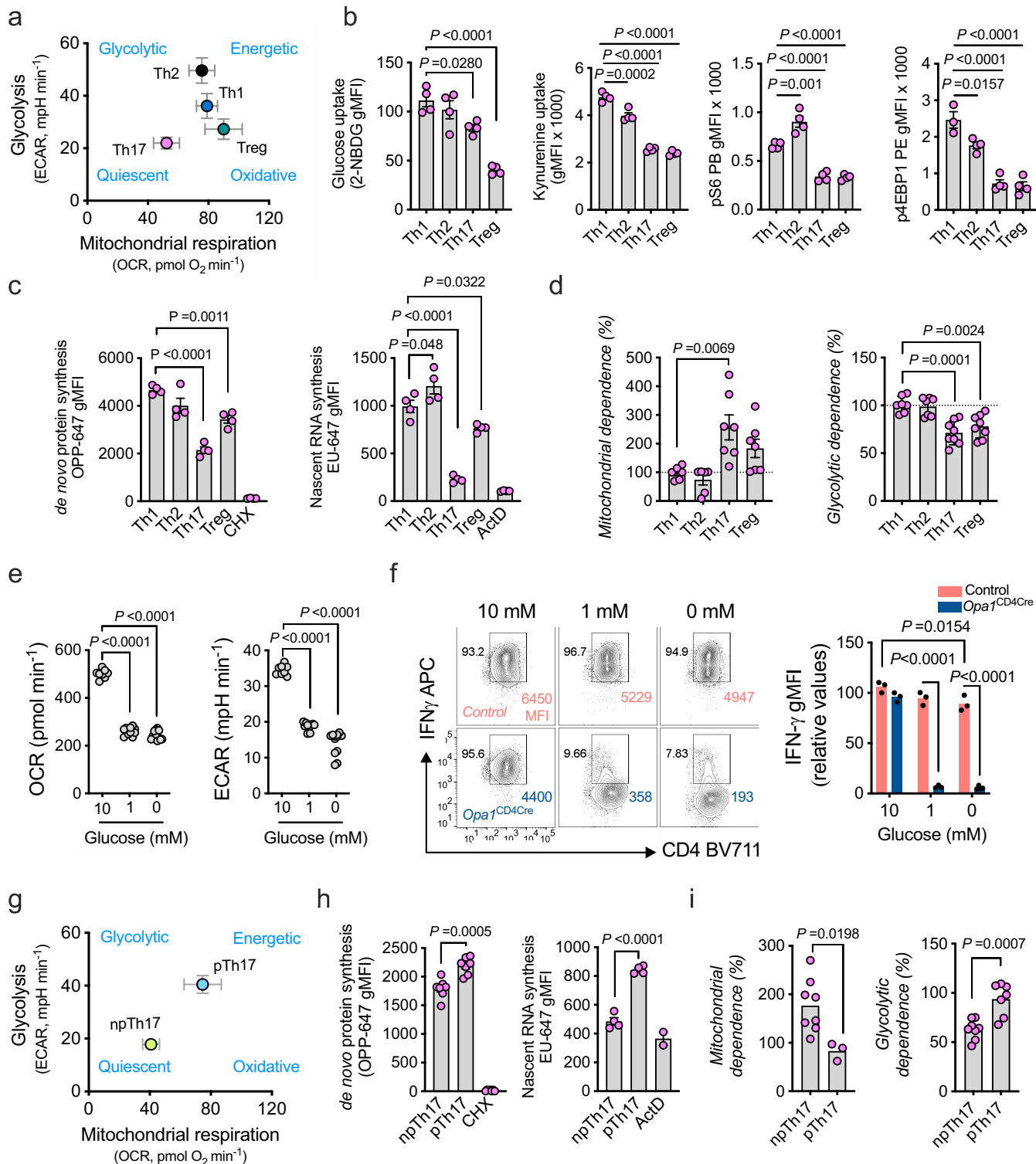
Extended Data Fig. 5 | Th17 cells rely on OPA1 independent of metabolic activity. ***a***, ***b***, ***c***, ***d***, CD4⁺ T$_N$ cells were cultured in Th and Treg conditions. **a)** Bioenergetic profile (baseline OCR/ECAR, $n = 4$ independent experiments). **b)** Glucose and kynurenine uptake, phosphorylated S6 ($n = 4$) and 4E-BP1 (Th1: $n = 3$, Th2,Th17,Treg: $n = 4$ biological replicates). **c)** *de novo* protein and nascent RNA synthesis by O-propargyl puromycin (OPP) and ribonucleoside ethynyl uridine (EU) incorporation, respectively ($n = 4$ biological replicates). Cyclohexamide (CHX) and actinomycin D (ActD): negative controls. **d)** Protein translation dependence on mitochondria (*left*, Th1, Th2: $n = 6$; Th17,Treg: $n = 7$ biological replicates) or glycolysis (*right*, Th1, Th2: $n = 7$: Th17, Treg: $n = 8$ biological replicates), 2 independent experiments. (**e**) OCR and ECAR (10 mM: $n = 8$; 1 mM and 0 mM $n = 4$ biological replicates) and (**f**) IFN-γ expression ($n = 3$

biological replicates) in cells cultured in Th1 conditions 3 days before overnight culture in RPMI with 10% non-dialyzed FBS and decreasing glucose concentrations. ***g***, ***h***, ***i***, CD4⁺ T$_N$ cells cultured in Th17 np/p conditions. **g)** Bioenergetic profile ($n = 4$ biological replicates). **h)** *de novo* protein synthesis (*left*, $n = 7$ biological replicates, 2 independent experiments) and nascent RNA synthesis (*right*, np/p: $n = 4$, ActD: $n = 2$ biological replicates). **i)** Protein translation dependence on mitochondria (*left*, np: $n = 8$: p: $n = 3$ biological replicates) or glycolysis (*right*, np: $n = 8$: p: $n = 7$ biological replicates, 2 independent experiments). Representative plots and graphs summarize results of at least two independent experiments, except where noted otherwise. Data are means ± s.e.m. Two-sided Tukey's test (**b**–**e**), Šidák's test (**f**) or unpaired two-tailed *t*-test (**h**, **i**). Exact *P* values are indicated.
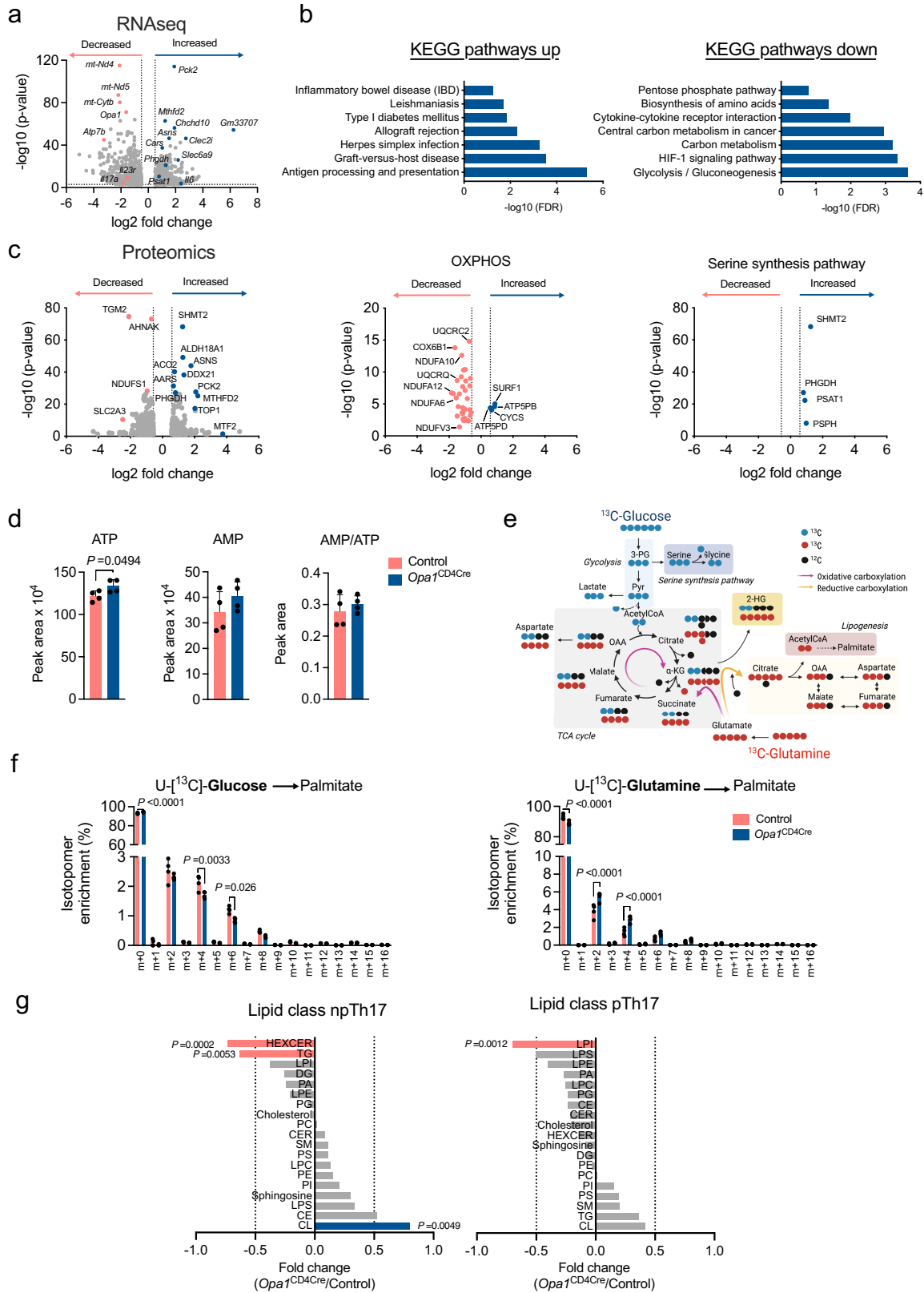
Extended Data Fig. 6 | See next page for caption.

Extended Data Fig. 6 | Multi-OMICS analysis of Th17 cells upon OPA1 deletion. Control and *Opa1*[CD4Cre] CD4^{+} T_N cells were cultured in Th17 conditions and the RNA extracted and sequenced. **a**) Volcano plot shows differentially expressed genes (1518: log10 *P* value < 3, log2 FC > 0.5). **b**) DAVID KEGG pathway analysis from differentially up- (779) or downregulated (739) genes (FDR, false discovery rate). **c**) Control and *Opa1*[CD4Cre] CD4^{+} T_N cells were cultured in Th17 conditions and proteins from whole cell lysates extracted and analyzed (LC-MS). *Left*, volcano plot from differentially expressed proteins (562: log10 *P* value<1.3, log2 FC > 0.58). *Middle* and *right* volcano plots, protein expression in relation to OXPHOS and serine and glycine biosynthesis pathways, respectively. **d**) Cellular ATP, AMP and AMP/ATP ratio by LC-MS (*n* = 4 per genotype, day 4). **e**) Schematic of [U-13C]-Glucose and [U-13C]-Glutamine carbon allocation into central carbon metabolites. **f**) Fractional labelling of palmitate with [U-13C]-Glucose (*left)* or [U-13C]-Glutamine (*right*) in control and *Opa1*[CD4Cre] Th17 cells cultured 20 *h* on day 3 with fully labelled subsrates (*n* = 4 per group). **g**) Control and *Opa1*[CD4Cre] CD4^{+} T_N cells were cultured in Th17 conditions 4 days and lipids extracted and analyzed (*n* = 4 biological replicates). Graph, FC of distinct lipid classes in *Opa1*[CD4Cre] *vs.* control (HEXCER: hexosylceramide, TG: triacylglycerades, LPI: lysophosphatidylinositol, DG: diacylglycerol, PA: phosphatidic acid, LPE: lysophosphatidylethanolamine, PG: phosphatidylglycerol, Cholesterol, PC: phosphatidylcholines, CER: ceramides, SM: sphingomyelin, PS: phosphatidylserine, LPC: lysophosphatidylcholines, PE: phosphatidylethanolamine, PI: phosphatidylinositol, Sphingosine, LPS: lipopolysaccharide, CE: cholesterol esters, CL: cardiolipins). Transcriptomics, proteomics and lipidomics were performed once (**a**,**b**: *n* = 3; **g**: *n* = 4 biological replicates). Graphs summarize results of at least two independent experiments in **d**, **f**. Data are means ± s.e.m. Unpaired two-tailed *t*-test (**a**, **c**, **d**, **f**, **g**). Exact *P* values are indicated.

Article
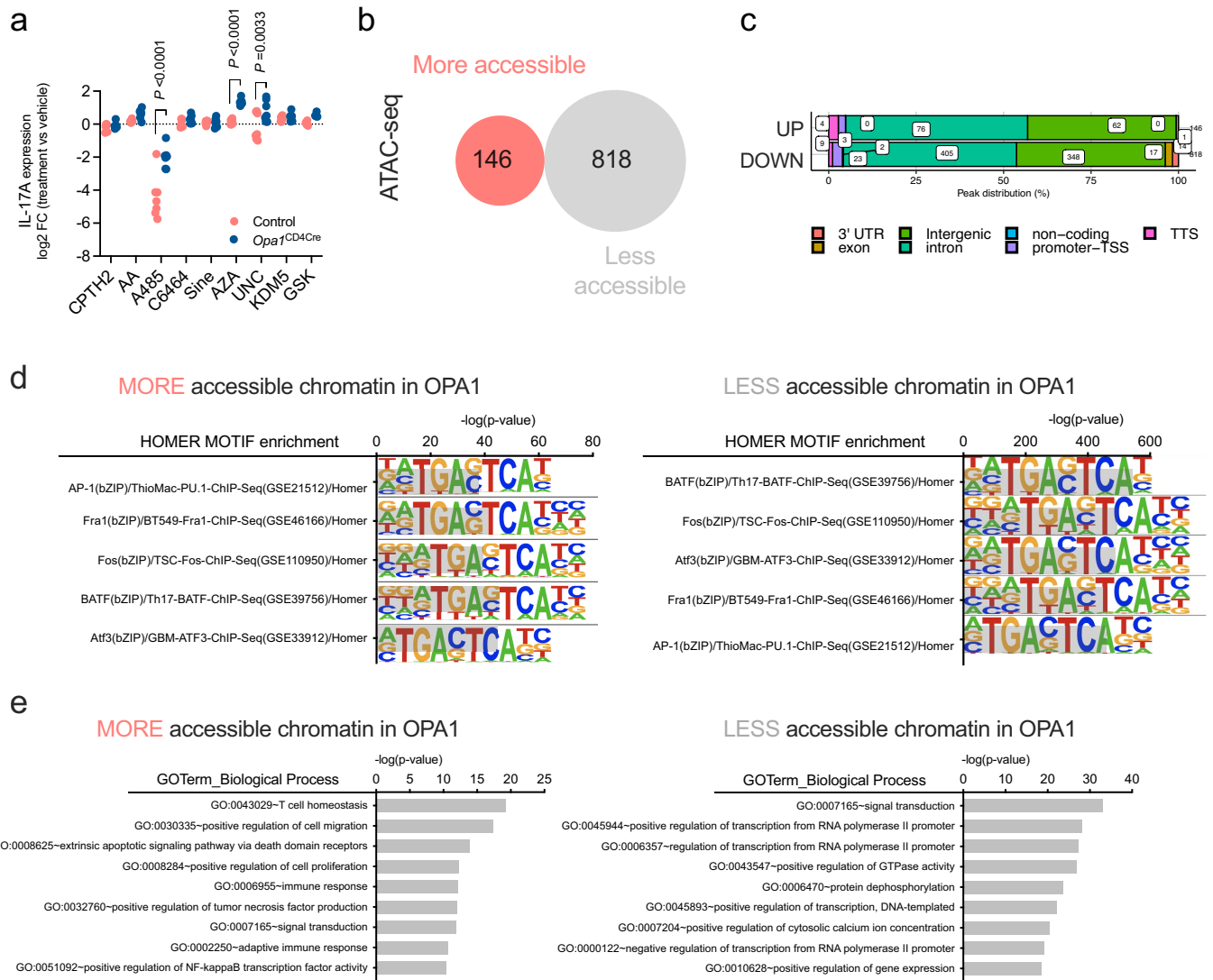
Extended Data Fig. 7 | OPA1 controls chromatin accessibility in Th17 cells.
a) CD4⁺ T_N cells from control and *Opa1*^CD4Cre mice were cultured in Th17
conditions for 1 day followed by 48 h incubation with inhibitors for histone
acetylation and methylation, and DNA methylation. IL-17A expression was
analyzed by flow cytometry and results show log2 FC of IL-17A MFI in
inhibitor-treated vs vehicle-treated cells (n = 7 biological replicates for all
conditions except GSK: n = 4 biological replicates). Graph combines data from
two independent experiments. Data are mean ± s.e.m. Two sided Šidák's test.

Exact P values are indicated. **b, c, d, e**, CD4⁺ T_N cells from control and *Opa1*^CD4Cre
mice were cultured in Th17 conditions 4 days and the DNA extracted and
processed for ATAC-seq (n = 3 biological replicates). **b**) Number of differentially
accessible chromatin regions (FC > 2, p < 0.01). **c**) Genomic localization of the
differentially regulated accessible chromatin regions. **d**) HOMER motif TF
analysis on regulated chromatin regions. **e**) GO term pathway enrichment
analysis from the differentially regulated accessible chromatin regions
between *Opa1*^CD4Cre and control Th17 cells (FC > 2, p < 0.01).
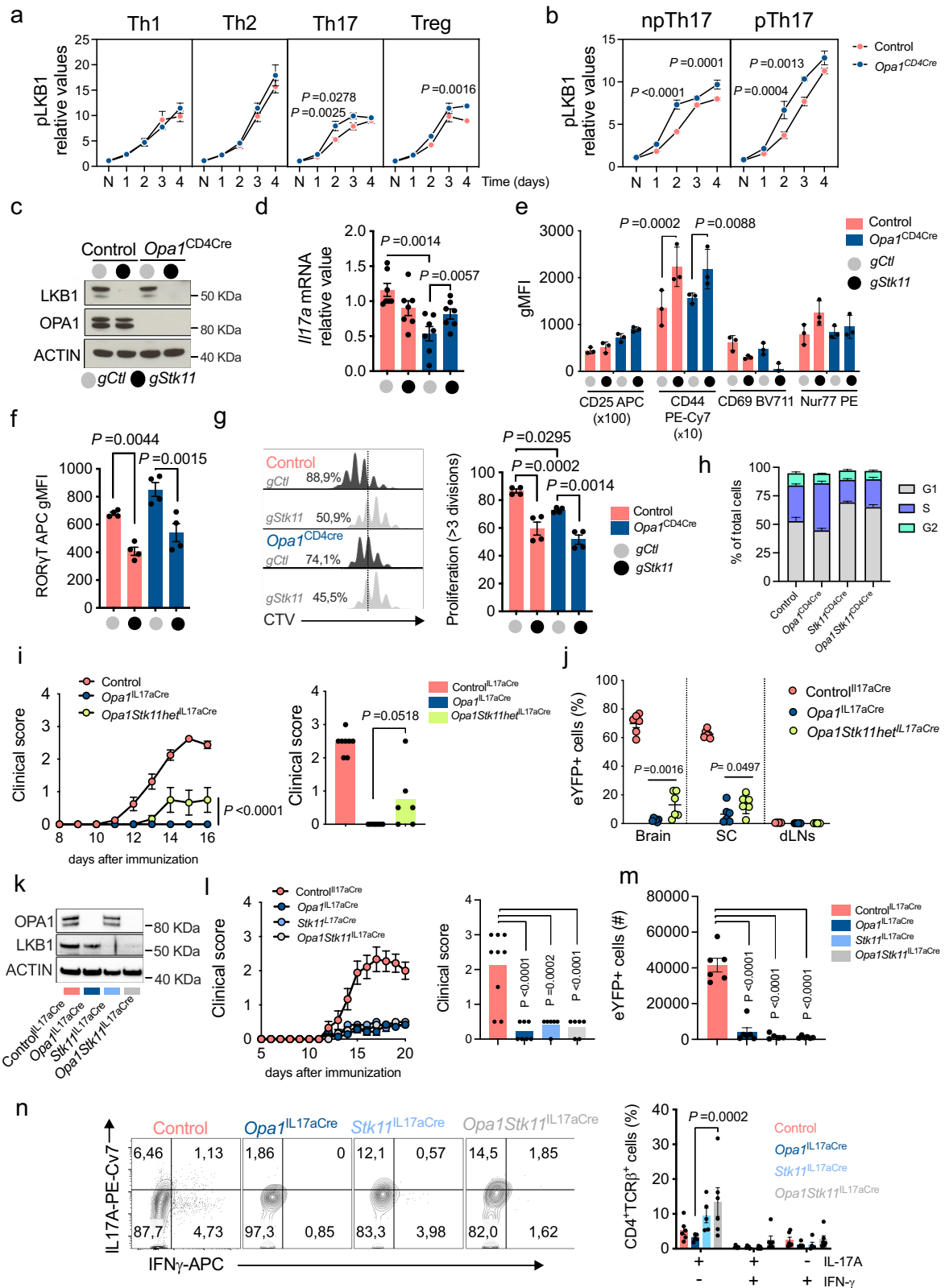
Extended Data Fig. 8 | See next page for caption.

Article

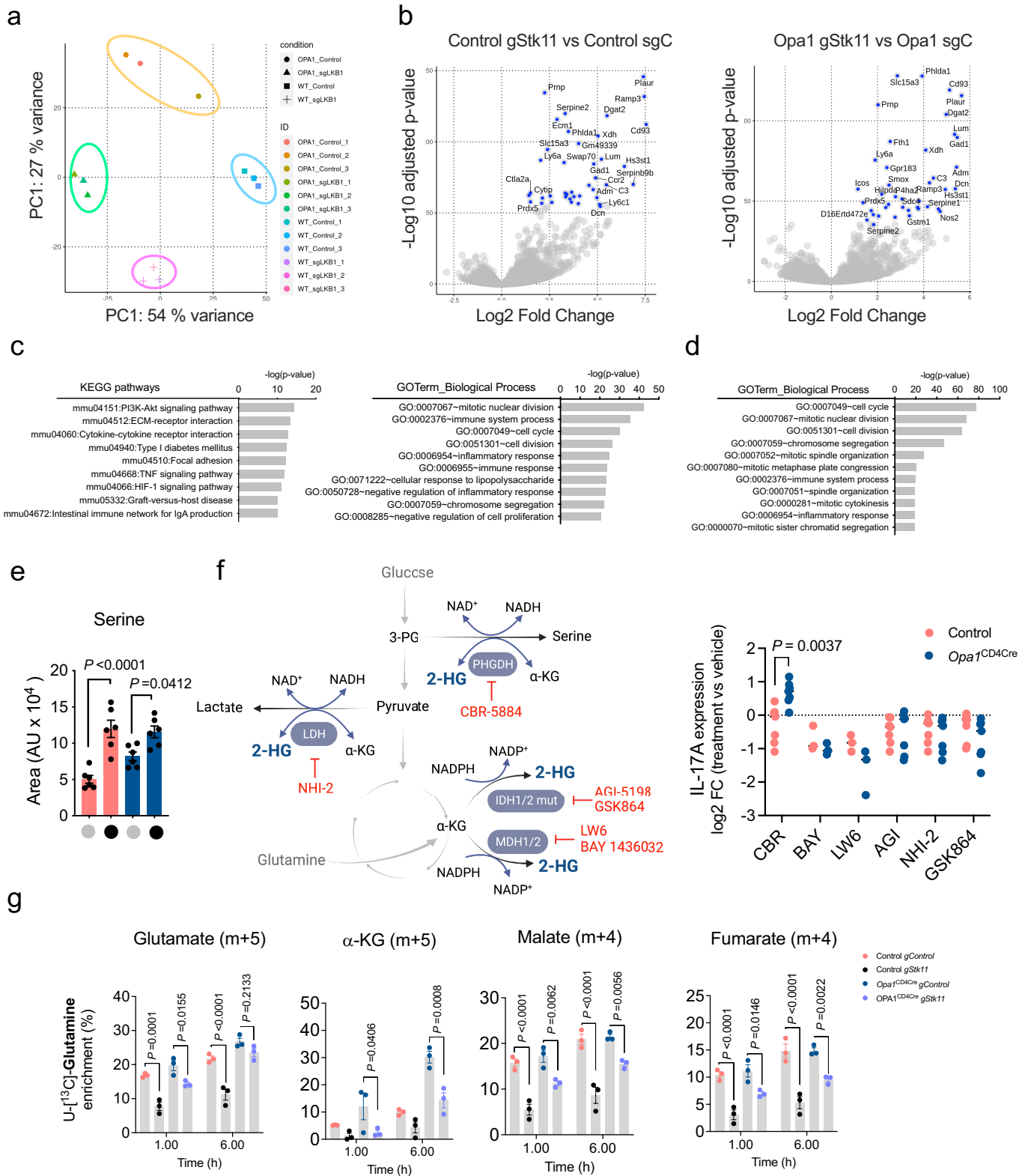**Extended Data Fig. 8 | LKB1 deletion in OPA1 reestablishes IL-17A expression.** LKB1 phosphorylation kinetics in CD4$^+$ T$_N$ cells cultured in Th and Treg (**a**) and np/p Th17 (**b**) conditions (Control: $n = 4$; $Opa1^{CD4Cre}$: $n = 3$ biological replicates). **c**, **d**, **e**, **f**, **g**, **h** Control and $Opa1^{CD4Cre}$ CD4$^+$ T$_N$ cells transfected with Cas9 and indicated gRNAs. (**c**) Immunoblot for LKB1 and OPA1. ACTIN: loading control, (**d**) IL-17A mRNA expression (RT-PCR, $n = 7$), (**e**) CD25, CD44, CD69 and Nur77 expression ($n = 3$), (**f**) ROR-γT expression ($n = 4$), (**g**) cell proliferation ($n = 4$), (**h**) and cell-cycle analysis ($n = 4$, biological and transfection replicates). **i**) *Left*, clinical disease score upon MOG immunization and at day 16 (*Right*), (control: $n = 8$; $Opa1^{IL17aCre}$: $n = 7$; and $Opa1Stk11het^{IL17aCre}$: $n = 6$ mice). **j**) CD4$^+$TCRβ$^+$eYFP$^+$ cell frequencies, day 20 post-immunization ($n = 6$ mice).

k) Immunoblot for LKB1 and OPA1 in CD4$^+$TCRβ$^+$eYFP$^+$ cells from control, $Opa1^{IL17aCre}$, $Stk11^{IL17aCre}$ and $Opa1Stk11^{IL17aCre}$ mice. ACTIN: loading control. **l**) *Left*, clinical disease score upon MOG immunization and at day 16 (*Right*) (control: $n = 9$; $Opa1^{IL17aCre}$: $n = 7$; $Stk11^{IL17aCre}$: $n = 6$ and $Opa1Stk11^{IL17aCre}$: $n = 6$ mice). **m**) CD4$^+$TCRβ$^+$eYFP$^+$ SC cell numbers ($n = 6$ mice per genotype except $Stk11^{IL17aCre}$: $n = 5$ mice) and **n**) IL-17A and IFN-γ expression, day 20 post-immunization (control: $n = 6$ mice; $Opa1^{IL17Cre}$: $n = 5$ mice; $Stk11^{IL17Cre}$: $n = 5$ mice; $Opa1Stk11^{IL17Cre}$: $n = 6$ mice). Representative plots and graphs summarize results of at least two independent experiments, except noted otherwise. Data are means ± s.e.m. Two-sided Šidák's test (**a**, **b**, **h**, **n**) or Tukey's test (**d**, **e**, **f**, **g**, **i**, **j**, **l**, **m**). Exact *P* values are indicated.
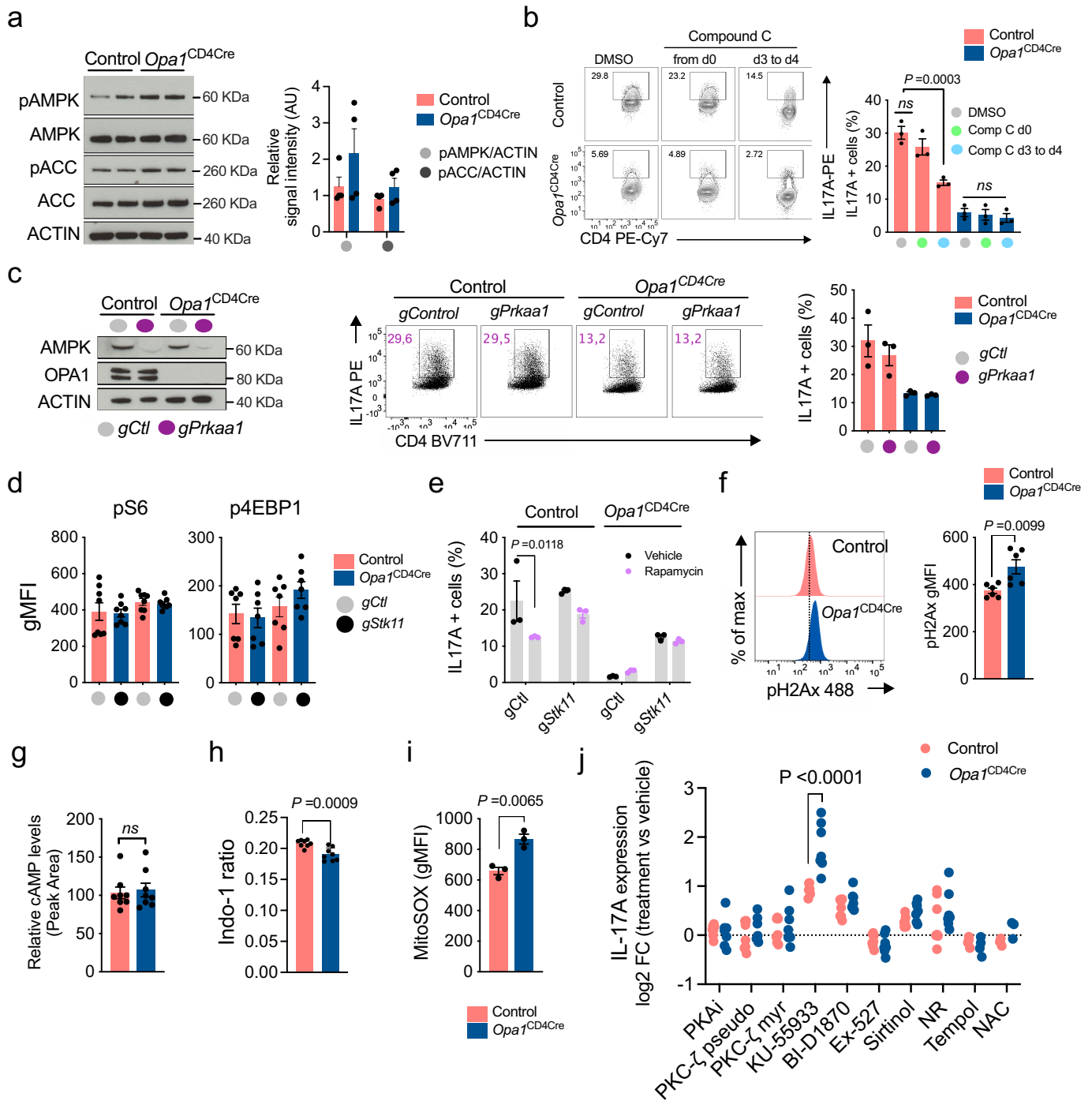
Extended Data Fig. 9 | LKB1 antagonizes OPA1 deficiency independent of mTOR and AMPK. a) Immunoblot for phosphorylated and total AMPK and ACC in control and *Opa1*[CD4Cre] Th17 cells. ACTIN: sample processing control. *Graph*, relative signal intensity (*n* = 4, 2 independent experiments). **b)** IL-17A expression in control and *Opa1*[CD4Cre] CD4^{+} T$_N$ cells cultured in Th17 conditions and Compound C from day 0 (d0) or from day 3 to 4 (d3) and restimulated (*n* = 3). **c)** *Left*, immunoblot for AMPK and OPA1 in T cells transfected with Cas9 and indicated gRNAs and cultured 5 days in Th17 conditions. ACTIN: sample processing control. *Right*, IL-17A expression in restimulated cells (*n* = 3 biological and transfection replicates). **d)** Expression of phosphorylated S6 (*n* = 8) and 4E-BP1 (*n* = 7 biological and transfection replicates), 2 independent experiments. **e)** IL-17A expression in T cells transfected with Cas9 and indicated

gRNAs and cultured in Th17 conditions 2 days followed by 48 *h* rapamycin treatment (*n* = 3 biological and transfection replicates). **f)** Phosphorylated H2Ax expression (*n* = 6, 2 independent experiments). **g)** Cyclic AMP (cAMP) levels (LC-MS, *n* = 8, 2 independent experiments). **h)** Basal calcium levels (*n* = 8, 2 independent experiments). **i)** Mitochondrial ROS (mitoSOX, *n* = 3). **j)** Control and *Opa1*[CD4Cre] CD4^{+} T$_N$ cells cultured in Th17 conditions 1 day followed by 2 day inhibitor-treatment. *Graph*, IL-17A MFI log2 FC inhibitor-treated *vs*. vehicle-treated cells (*n* = 7 biological replicates, except Tempol: *n* = 4 and NAC: *n* = 3, 2 independent experiments). Representative plots and graphs summarize results of at least two independent experiments, except noted otherwise. Data (**a**–**i**) are means ± s.e.m. Unpaired two-tailed *t*-test (**a**, **f**, **g**, **h**, **i**), two-sided Tukey's test (**b**, **c**, **d**) or Šidák's test (**e**, **j**). Exact *P* values are indicated.

a PC1: 27 % variance / PC1: 54 % variance

condition
- ● OPA1_Control
- ▲ OPA1_sgLKB1
- ■ WT_Control
- ✛ WT_sgLKB1

ID
- OPA1_Control_1
- OPA1_Control_2
- OPA1_Control_3
- OPA1_sgLKB1_1
- OPA1_sgLKB1_2
- OPA1_sgLKB1_3
- WT_Control_1
- WT_Control_2
- WT_Control_3
- WT_sgLKB1_1
- WT_sgLKB1_2
- WT_sgLKB1_3

b Control gStk11 vs Control sgC / Opa1 gStk11 vs Opa1 sgC

c KEGG pathways / GOTerm_Biological Process

d GOTerm_Biological Process

e Serine

f

g Glutamate (m+5) / α-KG (m+5) / Malate (m+4) / Fumarate (m+4)

Extended Data Fig. 10 | See next page for caption.

Extended Data Fig. 10 | LKB1 couples TCA cycle and serine metabolism to Th17 effector function. a) Principal component analysis (PCA) of the transcriptome of control and $Opa1^{CD4Cre}$ CD4$^+$ T$_N$ cells transfected with Cas9 and indicated gRNAs, cultured 4 days in Th17 conditions ($n = 3$ biological and transfection replicates). **b**) Volcano plots of the differentially expressed genes (DEG, FC > 1, p-value < 0.001) for the comparisons: control g$Stk11$ vs. control gCtl (*left*) and $Opa1^{CD4Cre}$ g$Stk11$ vs. $Opa1^{CD4Cre}$ gCtl (*right*). Blue dots annotate the highest 40 DEG. **c**, **d**, KEGG pathway and Gene Ontology (GO) annotation analysis from DEG (FC>1, p-value<0.001) between (**c**) control g$Stk11$ vs. control gCtl or (**d**) $Opa1^{CD4Cre}$ g$Stk11$ vs. $Opa1^{CD4Cre}$ gCtl. **e**) Intracellular serine in control and $Opa1^{CD4Cre}$ CD4$^+$ T$_N$ cells transfected with Cas9 and indicated gRNAs ($n = 6$ transfection replicates, 2 independent experiments) by LC-MS. **f**) *Left*, schematic shows 2-HG production from primary and promiscuous enzymatic

reactions and the inhibitors used for targeting its production. *Right*, CD4$^+$ T$_N$ cells from control and $Opa1^{CD4Cre}$ mice were cultured under Th17 conditions for 1 day followed by 48 h inhibitor treatment. IL-17A expression was analyzed by flow cytometry in restimulated cells and expressed as log2 FC inhibitor-treated vs. vehicle-treated cells (CBR, AGI, NHI-2, GSK864: $n = 7$ per group; BAY, LW6: $n = 3$ per group). Graph summarizes data from 2 experiments. **g**) Kinetics of fractional labelling of glutamate (m + 5), α-ketoglutarate (m + 4), malate (m + 4) and fumarate (m+4) in control and $Opa1^{CD4Cre}$ CD4$^+$ T cells transfected with Cas9 and indicated gRNAs cultured for 4 days in Th17 conditions and incubated with [U-^{13}C]-Glutamine for the indicated times ($n = 3$ biological and transfection replicates). Data are means ± s.e.m. Two-sided Šidák's test (**f**) or Tukey's test (**e**, **g**). Exact P values are indicated.

Corresponding author(s):   E.L. Pearce

Last updated by author(s):   Aug 1, 2022

Reporting Summary

Nature Research wishes to improve the reproducibility of the work that we publish. This form provides structure for consistency and transparency in reporting. For further information on Nature Research policies, see Authors & Referees and the Editorial Policy Checklist.

Statistics

For all statistical analyses, confirm that the following items are present in the figure legend, table legend, main text, or Methods section.

n/a	Confirmed	
☐	☒	The exact sample size (*n*) for each experimental group/condition, given as a discrete number and unit of measurement
☐	☒	A statement on whether measurements were taken from distinct samples or whether the same sample was measured repeatedly
☐	☒	The statistical test(s) used AND whether they are one- or two-sided *Only common tests should be described solely by name; describe more complex techniques in the Methods section.*
☒	☐	A description of all covariates tested
☐	☒	A description of any assumptions or corrections, such as tests of normality and adjustment for multiple comparisons
☐	☒	A full description of the statistical parameters including central tendency (e.g. means) or other basic estimates (e.g. regression coefficient) AND variation (e.g. standard deviation) or associated estimates of uncertainty (e.g. confidence intervals)
☐	☒	For null hypothesis testing, the test statistic (e.g. *F*, *t*, *r*) with confidence intervals, effect sizes, degrees of freedom and *P* value noted *Give P values as exact values whenever suitable.*
☒	☐	For Bayesian analysis, information on the choice of priors and Markov chain Monte Carlo settings
☒	☐	For hierarchical and complex designs, identification of the appropriate level for tests and full reporting of outcomes
☒	☐	Estimates of effect sizes (e.g. Cohen's *d*, Pearson's *r*), indicating how they were calculated

Our web collection on statistics for biologists contains articles on many of the points above.

Software and code

Policy information about availability of computer code

Data collection
: Bulk RNA-sequencing data was collected using deepTools v_2.0, STAR v_2.7.10, feature Counts v_2.0.3, DESeq2 v_1.36 and the Mus musculus genome assembly mm10. ATAC-sequencing data was collected using deepTools v_2.0, Trimmomatic v_0.4, Bowtie2 v_2.4.5, SAM tools v_1.4.1, MACS2 v_2.2.7.1, CSAW v_1.30.1, BedTools v.2.28.0, HOMER v_4.11 and the Mus musculus genome assembly mm10. Flow cytometry data was collected using LSR III Fortessa (BD Biosciences) and CytoFlex (Beckman Coulter). Glucose and glutamine tracing experiments (GC-MS) and metabolite quantification (LC-MS) data were collected using in-house R scripts that are publicly available (https://gitlab.gwdg.de/joerg.buescher/metabolomics_scripts.) Proteomics data was collected using Biognosys Spectronaut v_10.0 and MaxQuant v_1.6.1.0.

Data analysis
: RNA-sequencing data was processed in R using DESeq2 v_1.36 and visualized using Morpheus (Broad Institute). ATAC-sequencing data was visualized using IGV v_2.4.0. RNA-seq and ATAC-seq pathway analysis was performed using DAVID Software for Functional Annotation Bioinformatics Microarray Analysis (v 2016 and v 2021). Flow cytometry data was analyzed using Flowjo 10.7.2 (BD Biosciences). Proteomics data was analyzed using Biognosys Spectronaut v_10.0, MaxQuant software version 1.6.1.0. and the Mus musculus UniProt FASTA database (v2019). Proteomics pathway analysis was performed using Ingenuity Pathway Analysis (IPA, Qiagen). Lipidomics, LC-MS or GC-MS metabolomics data was analysed using MassHunter B.07.01, or in-house R code that is publicly available (https://gitlab.gwdg.de/joerg.buescher/ metabolomics_scripts). Data analysis and statistical analysis was performed using Prism 9 software (GraphPad) and Microsoft Excel (v16.46). Mitochondrial sphericity was determined with Imaris analysis software v_9.5 (Bitplane). Optical intensity signals in immunoblots and width of mitochondrial cristae from electron microscopy images were quantified with Image J software v_1.53c.

For manuscripts utilizing custom algorithms or software that are central to the research but not yet described in published literature, software must be made available to editors/reviewers. We strongly encourage code deposition in a community repository (e.g. GitHub). See the Nature Research guidelines for submitting code & software for further information.

Data

All manuscripts must include a data availability statement. This statement should provide the following information, where applicable:

- Accession codes, unique identifiers, or web links for publicly available datasets
- A list of figures that have associated raw data
- A description of any restrictions on data availability

RNA-seq and ATAC-seq data have been deposited in the Gene Expression Omnibus (GEO) as the superseries GSE207603. This superseries contains RNA-seq datasets with accession numbers GSE156742 and GSE207601 and a single ATAC-seq dataset with accession number GSE207602. The main data supporting the findings of this study are available within the article and its Supplementary Figures. Full scans of blots and source data are provided as Source data files.

Field-specific reporting

Please select the one below that is the best fit for your research. If you are not sure, read the appropriate sections before making your selection.

☒ Life sciences   ☐ Behavioural & social sciences   ☐ Ecological, evolutionary & environmental sciences

For a reference copy of the document with all sections, see nature.com/documents/nr-reporting-summary-flat.pdf

Life sciences study design

All studies must disclose on these points even when the disclosure is negative.

Sample size	No statistical methods were used to predetermine sample size. Sample sizes were determined based on the standard in the field, and on the numbers required to achieve statistical significance using indicated statistics. Replication between biological samples was robust, so at least 3 biological replicates were used for each experiment. Statistical analysis was consistent with the sample size of each experiment.
Data exclusions	If protein knockdown was not achieved during CRISPR-Cas9 experiments, the experiment was to be excluded. No exclusion criteria where established for the rest of the experiments.
Replication	All experiments were repeated at least twice and all repeats were successful.
Randomization	No randomization was performed for in vivo experiments, and experimental animals were analyzed along with age and sex-matched controls. For cell culture experiments, naive T cells were equally distributed into multi-well plates and the treatment condition was randomly applied. Additional controls for covariates were not performed, as mice were age- and sex-matched and T cells studied along genotypes or pharmacological treatments were activated and differentiated with the same specific conditions.
Blinding	Blinding was not relevant in this study, as groups consisted of previously genotyped mice in order to have correct experimental and control groups. Samples were standardized and were treated in exactly the same way prior to treatment, conditions were well-controlled, and the results are quantitative. All assessments were carried out using multiple independent replicates.

Reporting for specific materials, systems and methods

We require information from authors about some types of materials, experimental systems and methods used in many studies. Here, indicate whether each material, system or method listed is relevant to your study. If you are not sure if a list item applies to your research, read the appropriate section before selecting a response.

Materials & experimental systems

n/a	Involved in the study
☐	☒ Antibodies
☒	☐ Eukaryotic cell lines
☒	☐ Palaeontology
☐	☒ Animals and other organisms
☒	☐ Human research participants
☒	☐ Clinical data

Methods

n/a	Involved in the study
☒	☐ ChIP-seq
☐	☒ Flow cytometry
☒	☐ MRI-based neuroimaging

Antibodies

Antibodies used	The following antibodies were used for western blot: anti-β-actin (13E5, Cat# 4970S), anti-LKB1 (D60C5, Cat# 3047S), anti-phosphorylated LKB1 (Ser428, C67A3, Cat# 3482S), anti-AMPKα (D5A2, Cat# 5831S), anti-phosphorylated AMPKα (Thr172, 40H9, Cat #2535), anti-phosphorylated ACC (Ser79, Cat #3661), anti-ACC (C83B10, Cat #3676), anti-DRP1(D6C7, Cat# 8570), anti-

Tom20 (D8T4N, Cat#42406) and anti-MFN2 (D2D10, Cat#9482) from Cell Signaling, anti-OPA1 (18/OPA1, Cat# 612606) from BD Biosciences, anti-MFN1 antibody (EPR21953-74 Cat# ab221661) from Abcam, anti-Tubulin (DM1A, Cat#T9026) and anti-PHGDH (Cat# HPA021241) from Sigma, anti-PSPH (Cat#PA5-96863) from Thermo and anti-MTHFD2 (Cat# 12270-1-AP) from Proteintech. Secondary antibodies used were: Rabbit anti-Mouse IgG (H+L) Secondary Antibody, HRP, Cat#31450; and Goat anti-Rabbit IgG (H+L) Secondary Antibody, HRP, Cat#31460, from Thermofischer.

For flow cytometry, the antibody target and clone number are provided in the methods, and specific fluorochrome color is labeled in the figures.

Validation

All antibodies listed have been used in a number of previous publications, including ours. All antibodies are commercially available and have been validated in previously published studies:

anti-β-actin (13E5, Cat# 4970S, Cell Signaling). This monoclonal antibody detects β-actin and is validated in Human, Mouse, Rat, Monkey, Bovine and Pig. Reported in more than 4000 studies. https://www.cellsignal.com/products/primary-antibodies/b-actin-13e5-rabbit-mab/4970

anti-LKB1 (D60C5, Cat# 3047S, Cell Signaling). This monoclonal antibody detects total LKB1 protein. It is validated by manufacturer for WB in Human, Mouse, Rat, Monkey. Cited in more than 100 studies. https://www.cellsignal.com/products/primary-antibodies/lkb1-d60c5-rabbit-mab/3047

anti-phosphorylated LKB1 (Ser428, C67A3, Cat# 3482S, Cell Signaling). Detects LKB1 when phosphorylated at Ser428. It is validated by manufacturer for WB in Human, Mouse, Rat, Monkey. Cited in more than 90 studies. https://www.cellsignal.com/products/primary-antibodies/phospho-lkb1-ser428-c67a3-rabbit-mab/3482

anti-AMPKα (D5A2, Cat# 5831S, Cell Signaling). Detects AMPKα protein and is validated by manufacturer for WB. Detects AMPKα in Human, Mouse, Rat, Monkey and Bovine. Cited in more than 5500 studies. https://www.cellsignal.com/products/primary-antibodies/ampka-d5a2-rabbit-mab/5831

anti-phosphorylated AMPKα (Thr172, 40H9, Cat #2535, Cell Signaling). Rabbit mAb detects endogenous AMPKα only when phosphorylated at threonine 172. Validated for WB in a number of species, including Mouse. Cited in more than 2500 studies. https://www.cellsignal.com/products/primary-antibodies/phospho-ampka-thr172-40h9-rabbit-mab/2535

anti-phosphorylated ACC (Ser79, Cat #3661, Cell Signaling). This antibody detects endogenous levels of ACC only when phosphorylated at serine 79. Validated by manufacturer for WB in a number of species, including Mouse. Cited in more than 880 studies. https://www.cellsignal.com/products/primary-antibodies/phospho-acetyl-coa-carboxylase-ser79-antibody/3661

anti-ACC (C83B10, Cat #3676, Cell Signaling). This rabbit monoclonal antibody detects endogenous levels of all isoforms of acetyl-CoA carboxylase protein. Validated by manufacturer for WB in a number of species, including Mouse. Cited in more than 450 studies. https://www.cellsignal.com/products/primary-antibodies/acetyl-coa-carboxylase-c83b10-rabbit-mab/3676

anti-DRP1 (D6C7, Cat# 8570, Cell Signaling). This antibody recognizes endogenous levels of total DRP1 protein in Human, Mouse, Rat, Monkey. Validated by manufacturer for WB. Cited in more than 240 studies. https://www.cellsignal.com/products/primary-antibodies/drp1-d6c7-rabbit-mab/8570

anti-Tom20 (D8T4N, Cat#42406, Cell Signaling). This antibody recognizes Tom20 protein in Human, Mouse, Rat, Monkey. Validated by manufacturer for WB. Cited in more than 150 studies. https://www.cellsignal.com/products/primary-antibodies/tom20-d8t4n-rabbit-mab/42406

anti-MFN2 (D2D10, Cat#9482, Cell Signaling). This antibody recognizes total mitofusin-2 and is validated by manufacturer. Cited in more than 140 studies. https://www.cellsignal.com/products/primary-antibodies/mitofusin-2-d2d10-rabbit-mab/9482

anti-OPA1 (18/OPA1, Cat# 612606, BD Biosciences). This monoclonal antibody recognizes total OPA-1 and is validated by manufacturer for WB. Cited in more than 200 published studies. https://www.citeab.com/antibodies/2411667-612606-bd-transduction-laboratories-purified-mouse

anti-MFN1 antibody (EPR21953-74 Cat# ab221661, Abcam). This Rabbit monoclonal antibody recognizes total mitofusin-1 in Mouse and Rat and it is validated by manufacturer for WB. Cited in 2 publications. https://www.abcam.com/mitofusin-1-antibody-epr21953-74-ab221661.html

anti-Tubulin (DM1A, Cat#T9026, Sigma). This monoclonal Anti-α-Tubulin antibody produced in mouse has been used in western blot analysis and protein expression analysis. Cited in more than 4000 published studies. https://www.sigmaaldrich.com/CH/en/product/sigma/t9026

anti-PHGDH (Cat# HPA021241, Sigma). This polyclonal antibody detects PHGDH in Human, Mouse and Rat and it is validated by the Human Protein Atlas Project for WB. Cited in more than 40 published studies. https://www.sigmaaldrich.com/CH/en/product/sigma/hpa021241

anti-PSPH (Cat#PA5-96863, Thermo). This polyclonal antibody recognizes total PSPH in Human, Mouse and Rat and it is validated by manufacturer for WB. https://www.thermofisher.com/antibody/product/PSPH-Antibody-Polyclonal/PA5-96863

anti-MTHFD2 (Cat# 12270-1-AP, Proteintech). This polyclonal antibody recognizes total MTHFD2 in Human, Mouse and Rat and it is validated by manufacturer for WB. Cited in more than 25 published studies. https://www.ptglab.com/products/MTHFD2-Antibody-12270-1-AP.html

All antibodies from each supplier were tested prior to usage for analysis. Antibodies were titrated for proper amount based on manufactures instructions.

Animals and other organisms

Policy information about studies involving animals; ARRIVE guidelines recommended for reporting animal research

Laboratory animals

C57BL/6J (Stock no: 000664), PhAM (Stock No: 018397), CD4Cre (Stock No: 022071), IL17aCre (Stock No: 016879), Rosa26eYFP (Stock No: 006148), Great (IFN-g eYFP reporter, Stock No: 017581), 4Get (IL-4 EGFP reporter, Stock No: 004190), FIR (Foxp3 RFP reporter, Stock No: 008374), and conditional floxed Stk11 (Stk11flox Stock No: 014143) mice were purchased from The Jackson Laboratory. Opa1 and Drp1 conditional floxed mice were obtained from Dr. Hiromi Sesaki (Johns Hopkins University School of Medicine, Baltimore, MD). Mfn1 and Mfn2 conditional floxed mice were obtained from Dr. David C. Chan (California Institute of Technology, Pasadena, CA). All mice used in this study were housed and maintained under specific-pathogen-free conditions in ventilated cages in the animal facility of the Max Planck Institute for Immunobiology and Epigenetics (Freiburg, Germany). Cages were exposed to a 14h/10h light/dark cycle and the room temperature and humidity maintained and monitored. Food and water were provided ad libitum. 8-12 weeks old male and/or female mice, age-matched and sex-matched were used in the study.

Wild animals

No wild animals were used.

Field-collected samples

No field-collected samples were used.

Ethics oversight

All mice used in this study were housed and maintained under specific-pathogen-free conditions in the animal facility of the Max Planck Institute for Immunobiology and Epigenetics (Freiburg, Germany). All animal protocols were approved by the local animal care committee of the Regierungspraesidium Freiburg (Freiburg, Germany). This study was conducted in compliance with all relevant ethical regulations.

Note that full information on the approval of the study protocol must also be provided in the manuscript.

Flow Cytometry

Plots

Confirm that:

☒ The axis labels state the marker and fluorochrome used (e.g. CD4-FITC).

☒ The axis scales are clearly visible. Include numbers along axes only for bottom left plot of group (a 'group' is an analysis of identical markers).

☒ All plots are contour plots with outliers or pseudocolor plots.

☒ A numerical value for number of cells or percentage (with statistics) is provided.

Methodology

Sample preparation

Sample preparation is detailed in the materials and methods section. For in vitro T cell studies, naive CD4+ T cells were isolated from single cell suspensions obtained from spleen and peripheral lymph nodes (LN) from mice of the indicated genotypes. Single cell suspensions were incubated with biotinylated antibodies against mouse CD44, CD25, CD8, IgM, B220, CD19, Gr-1, MHC-II, F4/80, CD11c, CD11b and DX5 (Biolegend) in PBS 2% FCS 1 mM EDTA for 20 min at 4C, followed by negative selection using Streptavidin magnetic beads (Stem cell Technology). Naive CD4 T cells were activated as described in the methods section of the manuscript. For analysis of intracellular cytokine production and transcription factor (TF) expression, cells were collected on day 4 and reestimulated 6 h with phorbol myristate acetate (PMA, 50 ng ml-1) and ionomycin (1 ug ml-1) in the presence of Brefeldin A (Biolegend) for the last 4 h. Cells were washed with PBS 2% FCS 1 mM EDTA, incubated with LIVE/DEAD Fixable dye Blue (Thermo) and surface markers for 30 min with PBS 2% FCS 1 mM EDTA at 4C, washed and fixed and permeabilized with eBioscience Foxp3/Transcription Factor Fixation/Permeabilization Concentrate and Diluent as per manufacturer protocol. Staining for TF and cytokines was performed for 1 hour on ice in permeabilization buffer. Cells were then washed and analyzed in cytometers.
Further details for specific flow cytometry stainings and assays can be found in the Methods section.

Instrument

LSRII Fortessa (BD Biosciences) and CytoFlex (Beckman Coulter) flow cytometers

Software

All data was collected with FACS-DIVA (BD Biosciences) and CytExpert (Beckman Coulter) software. Data was analyzed using Flowjo 10.7.2 (Tree Star) software and graphs and statistical analysis performed with GraphPad Prism 9.

Cell population abundance

A small aliquot of sorted cells was collected and run on a cytometer to verify purity of the sorted samples. The aabundance of the relevant cell populations post-sorting 85-100% in experiments. In addition, cell counts were performed on samples post sort to verify correct cell numbers.

Gating strategy

For in vitro analysis of T cell cultures, cells were gated on FSC-a vs SSC-a, FSC-w vs SSC-w, FSC-h vs SSC-h to exclude doublets and FSC-a vs Live Dead to select live cells. CD4 T cells were identified by staining with CD4 and cytokine and transcription factor antibodies as stated on the methods section. A representative plot is found in Fig 1g.
To determine eYFP+ Th17 cells (CD4+/TCRbeta+) in vivo in IL17a-reporter animals, lymphocytes were cell surface stained with anti-CD45 (30-F11), anti-CD4 (A20), anti-TCRbeta (H57-597) from Biolegend and LIVE/DEAD Fixable dye Blue (Thermo) and

identified as CD45+/CD4+/TCRbeta+/eYFP+ cells. For detection of Th17 cells (CD4+/TCRbeta+) expressing eYFP in the central nervous system (CNS) of MOG-immunized mice, lymphocytes were cell surface-stained with CD45 (30-F11), CD11c (N418), CD4 (A20), anti-TCRbeta (H57-597) from Biolegend and LIVE/DEAD Fixable dye Blue (Thermo) and Th17 cells identified by expression of CD45+/CD4+/TCRbeta+/eYFP+. For intracellular detection of cytokines in cells from the small intestine or the CNS, lymphocytes were restimulated 4-5 h at 37°C in complete RPMI with PMA (50 ng ml-1, Sigma) and ionomycin (1 ug ml-1, Sigma) in the presence of Brefeldin A (1 ug ml-1,Sigma), cell surface stained, fixed with 2 % PFA 10 min at room temperature, and stained intracellularly with IL17A-PE (TC11-18H10.1) using the BD CytoFix/CytoPerm kit (BD Biosciences). A representative plot is found in Fig 2e.

☒ Tick this box to confirm that a figure exemplifying the gating strategy is provided in the Supplementary Information.